UNIVERSIDADE DE LISBOA

FACULDADE DE CIÊNCIAS

DEPARTAMENTO DE QUÍMICA E BIOQUÍMICA

Validation of voltage-gated sodium channels from dorsal root ganglia neurons as a pharmacological target for the treatment of Chronic pain

Mestrado em Bioquímica

Especialização em Bioquímica

Joana Maria Monteiro Serrão

Dissertação orientada pelo

Doutor Pedro A. Lima

2015

Acknowledgements

Ao meu orientador, Doutor Pedro Lima, por me ter acolhido na família que é o Laboratório de Fisiologia. Pela confiança e liberdade que me foi concedida no desenho experimental da dissertação e pela postura afável e motivadora ao longo de todo o ano.

À Doutora Marisa Sousa, ao André Bastos e à Clara Patrício pela amizade e ensinamentos.

Em particular à Marisa, um grande agradecimento pelo acompanhamento durante todo o ano e em especial nesta última fase.

Ao André, outro grande agradecimento pela paciência ao longo dos dias de eletrofisiologia e ajuda na análise de resultados.

À Clara, pela simpatia e disponibilidade dada, mesmo antes de tudo ter começado.

À Drª Angélica Roberto, pela realização das minuciosas cirurgias num dos modelos de dor.

À Professora Sílvia Conde e respetivos elementos da equipa, pela simpatia e acesso ao laboratório e equipamento para a quantificação de proteínas.

Ao Doutor Paulo Matos pelo acesso ao seu laboratório e equipamento para as experiências de imunohistoquímica.

À Catarina Pontes, pela amizade sempre presente, apesar da distância.

À minha irmã, pela postura exemplar e ao João, por me ter apresentado à Bioquímica e me ter apadrinhado.

Finalmente, aos meus pais, pelo apoio e compreensão ao longo do meu percurso académico, sem o qual nada disto seria possível.

Table of contents

Abbreviations

ASIC	Acid-sensing ion channel
ASO	Antisense Oligo Deoxynucleotides
ATP	Adenosine triphosphate
BCA	Bicinchoninic acid
BDNF	Brain-derived Neurotrophic Factor
BSA	Bovine Serum Albumin
Ca^{2+}	Calcium ion
CCI	Chronic Constriction Injury
CFA	Complete Freund's adjuvant
CGRP	Calcitonin Gene Related Peptide
CIP	Congenital Insensitivity to Pain
Cm	Whole-cell membrane Capacitance
CNS	Central Nervous System
CP	Chronic pain
DAPI	4',6-diamidino-2-phenylindole
DC	Dor crónica
DOC	Deoxycholate
DRG	Dorsal Root Ganglion
DTT	Dithiothreitol
E_{Na+}	Reversal Potential of Sodium
FBS	Fetal Bovine Serum
G	Conductance

GDNF	Glial Cell-derived Neurotrophic Factor
HB	Homogeneization Buffer
I	Current amplitude
IASP	International Association for the Study of Pain
IB4	Isolectin 4
IEM	Erythromelalgia
I-V	Current-Voltage relationship
J	Current Density
K^+	Potassium ion
L	Lumbar
LB	Lysis Buffer
mRNA	messenger Ribonucleic acid
Na^+	Sodium ion
Nav	Voltage-gated Sodium Channel
NGF	Neurotrophic Growth Factor
OCT	Optimal Cutting Temperature
PBS	Phosphate Buffered Saline
PEPD	Paroxysmal Extreme Pain Disorder
PIC	Protease Inhibitor Cocktail
PNS	Peripheral Nervous System
RMP	Rest Membrane Potential
Rpm	Rotations per minute
S	Sacral

SDS	Sodium dodecyl sulphate
SEM	Standard Error of the Mean
SNL	Spared Nerve Ligation
TBS	TRIS-buffered saline
TrkA	Tropomyosin receptor kinase A
TRP	Transient Receptor Potential Channel
TRPA	Transient Receptor Potential Channel, sub-family A - Ankyrin
TRPM	Transient Receptor Potential Channel, sub-family M -Melastin
TRPV	Transient Receptor Potential Channel, sub-family V -Vanilloid
TTX	Tetrodotoxin
Va	Voltage of activation
V_H	Voltage of half activation or inactivation
vFF	von Frey Filament
VGSC	Voltage-gated Sodium Channel
Vm	Voltage pulsed current
Vs	Slop constant
a_i	Exponential amplitude coefficient
τ	Time constant

Resumo

A capacidade de um indivíduo percecionar estímulos dolorosos é de extrema importância. Ao sentir ou associar uma situação a uma experiência dolorosa, o indivíduo pode adotar posturas protetoras, de forma a evitar possíveis danos causados pela situação eminente e/ou futuras situações semelhantes. Os mecanismos moleculares inerentes à deteção de estímulos (mecânicos, térmicos ou químicos) e capazes de codificar dor pelos neurónios sensoriais primários (nocicetores) integram o fenómeno de nociceção. Contudo, em situações fisiopatológicas, é possível que os doentes desenvolvam Dor crónica (DC), uma síndrome em que a perceção da dor é exacerbada e os doentes sofrem de hiperalgesia (reação exagerada a um estímulo doloroso), alodinia (sensação de dor a um estímulo não doloroso), dor espontânea, parestesia (sensação anormal) e disestesia (parestesia desconfortável).

A DC afeta mais de 20% da população Humana e as suas etiologias são variadas: trauma, doenças autoimunes e metabólicas, infeções, tratamento antirretroviral e quimioterapia. Apesar da grande incidência, atualmente não existe uma abordagem terapêutica eficiente que possa suplantar as necessidades dos doentes, o que agrava as consequências psicológicas, sociais e económicas desta patologia. Os atuais tratamentos farmacológicos variam entre anti-inflamatórios não esteróides, opióides, antidepressivos e anticonvulsivos que, para além de frequentemente não serem eficientes, estão associados a efeitos secundários indesejáveis como a dependência, habituação ou até mesmo a perda da capacidade de gestão da dor.

As fibras nervosas C e Aδ transmitem eletricamente os estímulos sensoriais, a velocidade de transmissão nas fibras C (0,5-2m^{-1}·s), devido à ausência de um revestimento de mielina, é consideravelmente mais lenta, comparando à velocidade de transmissão das fibras Aδ (6-30 m^{-1}·s). A perceção dos estímulos transmitidos pelas fibras C é difusa, ao passo que os transmitidos pelas fibras Aδ são percecionados como bem localizados.

Todas as fibras nocicetivas são constituídas pelos neurónios do gânglio da raiz dorsal (DRG, do inglês *Dorsal Root Ganglia*). Estes últimos são classificados de acordo com o seu diâmetro em pequeno (27-31µm), médio (31-40µm) e grande (40-50µm); e

possuem uma anatomia pseudounipolar, com um longo axónio que inerva a periferia do organismo e um axónio mais curto que se dirige para o corno da raiz dorsal da medula espinal e o corpo celular alojado em locais específicos no interior da coluna vertebral. Os conjuntos dos corpos celulares destes neurónios é então designado de gânglio da raiz dorsal e a sua localização dentro da coluna vertebral é específica às fibras aferentes correspondentes. Dado o foco da presente dissertação, será dada uma especial atenção aos neurónios-DRG de pequeno e médio diâmetro integrantes da nociceção, que compõem as fibras C e Aδ, respetivamente.

Em situações fisiológicas, na ausência de estímulos capazes de produzir dor, os nocicetores encontram-se quiescentes, sem qualquer informação a ser transmitida. No entanto, na presença destes estímulos, os recetores nas terminações nervosas dos neurónios primários podem ser ativados. Quando o estímulo tem uma magnitude maior do que o limiar de ativação das fibras nervosas, é produzido um potencial de ação, que percorre a fibra nervosa, terminando nas lâminas I e II no interior do corno da raiz dorsal da medula espinal. A partir daí, a informação é transmitida para os neurónios secundários, para de seguida ser transmitida ao sistema nervoso central, onde no córtex sensorial do cérebro, a informação a relativa à quantificação e localização da dor é integrada.

A geração e transmissão de potenciais de ação é particularmente devida à ativação dos canais de sódio (Na^+) ativados pela voltagem (VGSC, do inglês *voltage-gated sodium channels*) presentes ao longo de todo o neurónio-DRG. Até à data estão identificadas nove isoformas diferentes de VGSC (Nav1.1-9), que diferem nas propriedades eletrofisiológicas e distribuição corporal. As isoformas Nav1.7, Nav1.8 e Nav1.9 encontram-se preferencialmente distribuídas nos neurónios-DRG responsáveis pela transmissão nocicetiva. Patologias relacionadas com a perda ou o ganho de função dos genes que codificam para o Nav1.7 e Nav1.8 estão associadas a anomalias na perceção de dor, nomeadamente hipo ou hipersensibilidade.

Ainda existe muito por se desvendar na fisiopatologia da DC, no entanto, sabe-se que os neurónios-DRG se encontram hiperexcitáveis neste contexto, comparativamente a situações fisiológicas. Estudos anteriores têm evidenciado

alterações nos canais iónicos ativados pela voltagem, nomeadamente VGSC, que levam a esse estado de hiperexcitabilidade nestes neurónios.

A estratégica terapêutica alternativa mais promissora para tratar DC visa a redução dessa "hiperexcitabilidade neural" que pode ocorrer através da alteração do funcionamento de canais-iónicos-chave que modulam a atividade elétrica desses neurónios. O conhecimento sobre as correntes iónicas subjacentes ao funcionamento de determinados canais é assim preponderante. Os canais/correntes especificamente implicados na DC carecem ainda de um conhecimento mais aprofundado e da sua validação como potenciais alvos terapêuticos.

A presente dissertação objetiva o estudo das características eletrofisiológicas das correntes de Na^+, com direta relevância para a DC em neurónios-DRG de pequeno diâmetro, através do estudo da biofísica e expressão destes canais.

Para tal, e uma vez que a DC pode ter várias etiologias, esta síndrome foi estudada no contexto de origem inflamatória e neuropática, baseando-se em modelos animais de dor em ratos. A DC inflamatória foi estudada através da indução de monoartrite no joelho do rato (ipsilateral), pela injeção de uma substância que ativa o sistema imunitário: *Complete Freund's Adjuvant* (CFA). No caso da dor neuropática, usou-se o muito comum modelo *Chronic Constriction Injury* (CCI), que assenta na constrição crónica do nervo isquiático do rato (ipsilateral), ao nível da coxa, através de quatro nós soltos em torno do mesmo realizados cirurgicamente.

O desenvolvimento de DC em ambos os modelos foi acompanhado ao longo do tempo através de testes comportamentais. Estes testes permitiram a observação do aparecimento de posturas putativas de evidenciarem dor espontânea em ratos. Foi também realizado o estudo do desenvolvimento de hiperalgesia, através da observação de reflexos protetores quando os ratos eram submetidos a estímulos mecânicos aplicados na pata e da alodinia ao frio, quando era aplicada acetona também na pata. No modelo inflamatório foi observada uma maior sensibilidade nos primeiros dias após a indução de dor, tendo os ratos apresentado uma recuperação parcial da sensibilidade no final do tempo de progressão do modelo. No modelo

neuropático, os ratos modelo desenvolveram hiperalgesia durante o curso da experiência, durante o qual também desenvolveram alodinia ao frio.

Ao fim de 21 e 28 dias após a indução de dor, nos modelos inflamatório e neuropático, respetivamente, os ratos foram sacrificados e os DRGs, foram coletados para futuras experiências.

As propriedades biofísicas das correntes de Na^+ foram estudadas por registos eletrofisiológicos em neurónios-DRG de pequeno diâmetro isolados, obtidos a partir de preparações *ex-vivo* de ratos controlo e dos modelos de DC. No estudo da DC inflamatória não se observaram diferenças significativas entre as correntes de Na^+ provenientes de neurónios de ratos controlo e de dor. No entanto, no caso do estudo da dor neuropática, observaram-se algumas tendências: a densidade da corrente de Na^+ que flui pela área membrana celular é maior nos neurónios-DRG provenientes dos ratos CCI e o tempo que essas mesmas correntes demoram a recuperar a sua magnitude após a inativação dos VGSC é também menor. Estas alterações biofísicas podem ser a razão pela qual, no contexto de DC, os neurónios encontram-se hiperexcitáveis e conseguem suportar uma maior frequência de disparo dos potenciais de ação. É importante referir que trabalhos anteriores demonstraram que o Nav1.8 é a isoforma presente em situações fisiológicas nos pequenos neurónios DRG, com um perfil eletrofisiológico que mais se adequa a estas alterações observadas.

Paralelamente, a expressão proteica dos canais de sódio Nav1.7 e Nav1.8 foi comparada entre os gânglios do lado ipsilateral (sujeitos ao modelo de dor) e do lado contralateral (controlo interno) à indução de dor. Pela análise por *Western blot,* observou-se um aumento da expressão de Nav1.7 e Nav1.8 nos gânglios ipsilaterais dos ratos com dor neuropática (CCI). Por análise imunohistoquímica, observou-se que estes canais são expressos nos neurónios DRG e que poderá existir um aumento da expressão de Nav1.7 nos gânglios do lado ipsilateral no modelo inflamatório (CFA), quando comparados com os gânglios contralaterais.

Em resumo, a presente dissertação permitiu observar que neurónios-DRG de pequeno diâmetro sofrem alterações na DC, nomeadamente nas propriedades biofísicas e de expressão dos VGSC.

No futuro serão necessários mais ensaios eletrofisiológicos que discriminem dentro das correntes totais de Na^+, quais as isoformas dos VGSC presentes nos neurónios DRG que induzem a modificações na sua excitabilidade. Deste modo, poder-se-á compreender quais os padrões-tipo de atividade bem como as diferenças a nível funcional dos neurónios provenientes de ratos com dor comparativamente aos controlos. Serão também necessárias mais análises de expressão dos VGSC nos DRGs destes modelos de dor, para um melhor entendimento das tendências observadas.

Deste modo, espera-se que uma mais consistente validação dos neurónios DRG como alvo farmacológico e, em particular dos VGSC por estes expressos, tragam informações relevantes para o desenvolvimento de novas terapias para a DC. Idealmente, o fármaco permitiria aos pacientes a recuperação da excitabilidade fisiológica destes neurónios, sem atuar no sistema nervoso central, evitando efeitos secundários indesejáveis e conferido aos pacientes uma melhor qualidade de vida.

Palavras-chave

Dor crónica; canais de sódio ativados pela voltagem; novo alvo terapêutico; neurónios do gânglio da raiz dorsal; comportamento animal.

Abstract

Chronic pain (CP) affects 21% of the human population and to date there is still no adequate treatment for this syndrome. Previous studies have indicated dorsal root ganglia (DRG) neurons, as crucial for the transmission of pain stimulus. The activity of these neurons leads to brain perception of pain, which is found to be exacerbated in CP patients. Such condition derives from the abnormal function of pivotal ion channels that shape the electric activity in DRG neurons. Therefore, the most promising therapeutic approach for CP relies on reducing this neuronal hyperexcitability.

In this regard, voltage-gated Sodium channels (VGSC) have the ability to initiate the electrical signalling in excitable cells, a characteristic that makes them potential drug targets. The peripheral localization of DRG neurons and its preferential expression of the Sodium channel isoforms Nav1.7, Nav1.8 and Nav1.9, makes them key targets for the development of novel analgesics to treat CP. Nevertheless, there is still a great demand for novel functional studies of those currents/channels sub-types specifically involved in the processes of CP, namely neuropathic and inflammatory pain.

The aim of this project was to study alterations in VGSC currents/channels in DRG neurons from rat models of neuropathic and inflammatory CP; specifically, to identify the biophysical and pharmacologic patterns that change following CP and correlating those with animal behaviour tests.

Overall, results show development of hyperalgesia and an abnormal function and expression of VGSC in DRG neurons following neuropathic pain in rat models, contributing to the validation of VGSC in DRG neurons as potential targets for novel analgesics in CP.

Keywords

Chronic pain; Voltage-gated sodium channels; novel therapeutic target; dorsal root ganglia neurons; animal behaviour.

1. Introduction

1.1 Nociception

Sensory signals are present in our lives as a way for us to perceive the environment. The molecular mechanisms inherent to the detection of pain-producing stimuli by the primary sensory neurons (nociceptors) constitute the components of nociception (Julius 2001). Events occurring outside are perceived as different sensory events recruiting distinct receptors and pathways that lead information to the brain, Figure 1 (Basbaum et al. 2009).

Nociception is initiated in the primary afferent neurons from the peripheral nervous system (PNS). In their terminals, primary afferent neurons have nociceptive transducers and ion channel complexes that are activated by irritant chemical, noxious heat or cold or mechanical stimuli (Basbaum et al. 2009). In physiological conditions, in the absence of a noxious stimuli, nociceptors are in a quiescent state and no information is transduced (Brouwer et al. 2014).

Figure 1 – *René Descartes, 'The Path of Burning Pain', 1664*. This was one of the first works establishing a link between pain perception and the brain, rather than the previous assumption that pain would be a spiritual, mystical experience.

The stimulation of the receptors from nociceptors may trigger voltage-gated calcium (Ca^{2}) and sodium (Na^{+}) channels present at the terminals of nerve fibers to initiate an action potential (AP), by which sensory information is transduced. All stimuli are codified and transduced through stereotyped electrical signals, virtually identical in all nerve cells. However, rather than the amplitude or frequency of those electrical signals transduced, perception is due to the connections of the neurons involved in the electrical transmission; and while the amplitude of coding doesn't confer any information, its frequency transmits the intensity of the stimuli (Nicholls et al. 1992).

If the initial stimulus is strong enough to trigger AP initiation, the generated AP travels the length of nerve fibers from their terminals to the next neuron. It passes to the cell body at the dorsal root ganglia (DRG), in the case of an afferent from the body, or at the trigeminal ganglia, when it comes from the face, and sequentially synapses with the secondary sensory neurons at the dorsal horn of the spinal cord, releasing neurotransmitters such as glutamate or substance P (Basbaum et al. 2009; Waxman & Zamponi 2014)

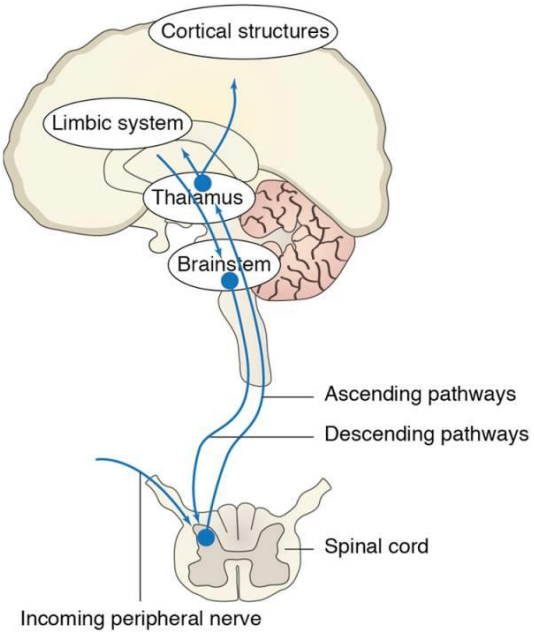

As demonstrated in Figure 2, the secondary neurons cross the midline of the spinal cord and ascend through the ventral and lateral spinothalamic tract to the medial and ventrobasal nuclei of the thalamus. The cells from the nuclei project to the somatosensory cortex and other areas of the nervous system - at this stage, one can localize the pain. An appropriate response is generated and transmitted through the descending pathways of the PNS (Nicholls et al., 1992).

Figure 2 – Transduction of peripheral stimuli to the brain. The incoming peripheral nerve synapses with the secondary neurons at the dorsal horn of the spinal cord and information is transduced by the ascending pathways of the spinal cord. The secondary neurons passes through the brain stem and delivers the information to the neurons at the thalamus, to be further transmitted to the somatosensory cortex and limbic system. An appropriate response is generated in the brain and transduced through the descending pathways of the PNS. Reproduced from O'Neill et al. 2012.

1.1.1 Noxious stimuli receptors

Nociceptors respond to different types of noxious stimuli through activation of specific receptors in their free nerve endings. The nature of those stimuli may be noxious heat (near 43°C), cold (below 15°C), chemical, or mechanical (Basbaum et al. 2009; Dai 2015).

The transient receptor potential (TRP) channels are a family of nonselective cation channels, wherein some are responsible for the transduction of internal or external noxious stimuli. The subfamily of Vanilloid receptors (TRPV1 to TRPV4) transduce noxious heat stimuli; from the Melastin (TRPM) family, the TRPM8 transduce noxious cold stimuli, as the TRPA1, from the Ankyrin family, that is also sensitive to low pH (Clapham 2003). The mechanisms associated to mechanotransduction and associated molecules are not fully understood to date (McCarter & Levine 2006), although there might be some candidates for mechanotransducers such as the acid-sensitive ion channels ASIC 1, 2 and 3 or the TRPA1 channel (Basbaum et al. 2009).

Activation of transducer receptors leads to an inward current of Ca^{2+} that depolarizes the cell membrane potential, if the depolarization is large enough to activate the voltage-gated Na^{+} channels (VGSC), an AP is generated and stimuli information is transduced to the brain (Waxman & Zamponi 2014).

Repeated stimulation of nociceptors may lead to progressive increase in the response from primary and secondary neurons, by a process called sensitization (Woolf & Salter 2000). Special attention will be given to the sensitization of nociceptors under the section *1.2 Pain*, due to the scope of the present work.

1.1.2 Nerve fibers

After the activation of the transducers at the free nerve endings and generation of an AP, the electrical signals are then transmitted through nerve fibers, classified according to their conduction velocity, as depicted in Table 1. The Aα-fiber is associated to motor and skeletal muscle functions, while the Aβ-fibers are typically associated to proprioception and low-threshold mechanoreception, furthermore, Aδ-fibers and C-fibers are associated to nociception (Harper & Lawson 1985; Rush et al. 2007; Ho & O'Leary 2011). The C-fibers have a much slower conduction velocity compared to A-fibers (*see Table 1*), because unlike the former, C-fibers are not myelinated (Snell 2006).

Table 1 – Classification of nerve fibers and principal features. Adapted from Snell, 2006.

Fiber Type	Conduction velocity ($m^{-1} \cdot s$)	Fiber diameter (μm)	Functions	Myelin
Aα	70-120	12-20	• Motor • Skeletal muscle	Yes
Aβ	40-70	5-12	• Sensory • Touch • Pressure • Vibration	Yes
Aδ	6-30	2-5	• Pain (sharp, localized) • Temperature • Touch	Yes
C	0.5-2	0.4-1.2	• Pain (difuse, deep) • Temperature • Postganglionic autonomic	No

Furthermore, C-fibers are divided in peptidergic and non-peptidergic subpopulations. The peptidergic C-fibers are isolectin 4 (IB4) negative and express neurothrophic growth factor (NGF)-dependent neuropeptides, such as substance P and calcitonin gene related peptide (CGRP), as well as NGF-receptor Tropomyosin receptor kinase A (TrkA) (Fukuoka & Noguchi 2011; Wang et al. 2007). The non-peptidegic C-fibers express the tyrosine kinase receptor c-ret, for the glial cell derived neurotrophic factor (GDNF) moreover, some of the c-ret positive C-fibers are also IB4 positive. (Basbaum et al. 2009)

The nociceptive nerve fibers and their connections within the dorsal horn are represented in Figure 3, the peptidergic C-fibers project to lamina I and outer lamina II of spinal dorsal horn, whilst the non-peptidergic C-fibers terminate in the inner part of lamina II. Furthermore, the Aδ-fibers terminates in the lamina II and V of the dorsal horn (Dib-Hajj et al. 2012; Fukuoka & Noguchi 2011). Finally, the large mechanosensor fibers sprout to the laminae III and V of the dorsal horn (Belkouch et al. 2014).

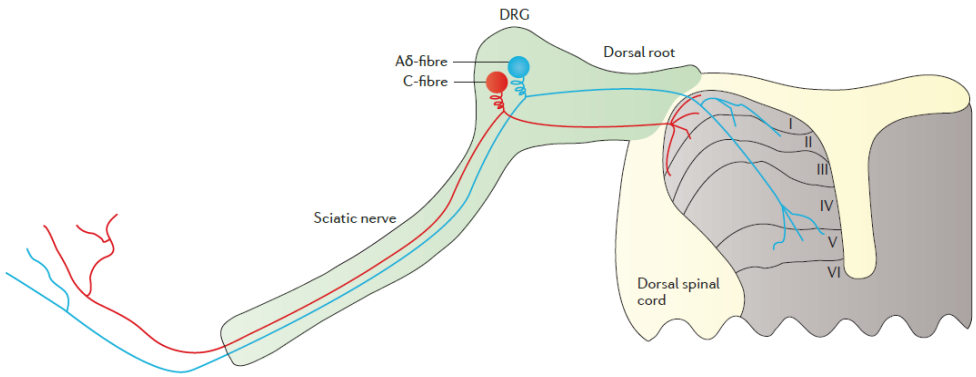

Figure 3 – Nociceptive nerve fibers. Noxious signals originated from the periphery are transmitted by the non-myelinated C-fibers (red) and Aδ-fibers (blue) to the secondary neurons in the dorsal horn of the spinal cord. C-fibers project to the nociceptive laminae I and II of the dorsal horn, whilst the Aδ-fibers projects to the lamina II and V of the dorsal horn. Reproduced from Dib-Hajj et al. 2012.

Due to the differences in action potential conduction and physiology of nerve fibers, the pain transmitted by Aδ-fibers is called “fast sharp pain” and it is well localized, whereas the pain transmitted by C-fibers is more diffuse and is called “slow pain” (Basbaum et al. 2009).

1.1.3 Dorsal Root Ganglia neurons

The DRG structure is a spherical collection of cell bodies from the afferent sensory fibers enervating the body, situated between adjacent vertebrae, represented in Figure 4. The location of a DRG is associated to their afferent fiber correspondent (Rush et al. 2007). In rats, the DRG inside the left and right side of the lumbar vertebrae L4 to L5 or to L4 to L6, depending on the rat strain, corresponds to the sciatic nerve from the left and right leg, respectively (Rigaud et al. 2008). However, in humans, the same nerves corresponds to DRG from the lumbar L4 to the sacral S3 vertebrae from the left and right sides of the body (Snell 2006).

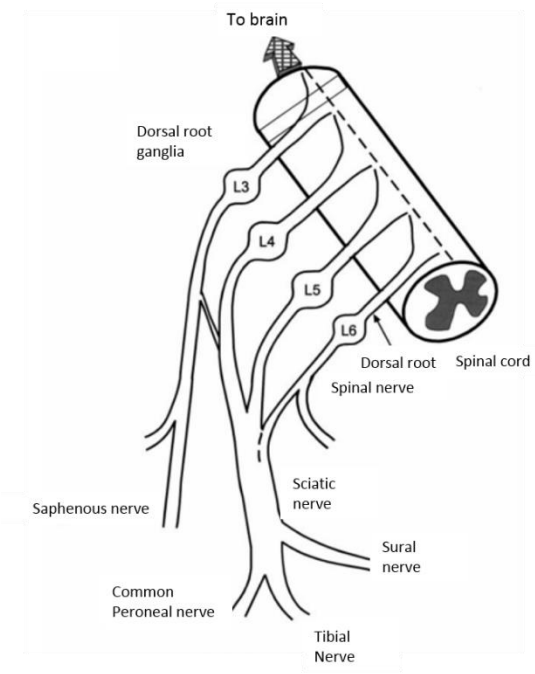

Figure 4 – Anatomy of the sciatic nerve from wistar rats. The DRG adjacent to the lumbar vertebra L4 to L6, called DRG L4-L6 have their afferents connected, forming the sciatic nerve. At the level of the mid-tight, named the sciatic notch, the nerve is divided in three branches (common peroneal, tibial and sural nerves) that enervate the leg and hind paw. Adapted from Decosterd & Woolf 2000.

The DRG neurons have a pseudounipolar anatomy, represented in Figure 5. Their axon is divided into two separate branches, a longer one from the periphery to the cell body and a smaller one from the cell body to the spinal cord, connected to the soma by a common axonal stalk, having the form of a T-stem axon. The ensemble of the cell bodies from an afferent nociceptive nerve constitutes the DRG (Krames 2014).

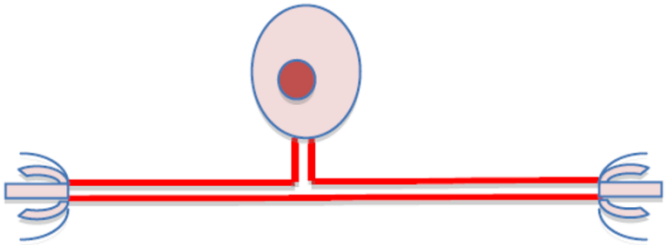

Figure 5 – Anatomy of a pseudounipolar neuron. Nociceptors have a pseudounipolar anatomy, their axon is divided in two branches and connected to the soma by a T-stem axon. One branch is evervating the target organ and the other is envervating the spinal cord; their soma is ensembled together with the soma of other nociceptors that constitute the same nerve fiber, forming the DRG. Adapted from Krames 2014.

DRG neurons are classified according to their soma diameter into large, medium and small diameter DRG neurons. Large diameter (40-50µm) DRG neurons are associated to Aβ-fibers and transduce vibratory and position sensation (Hong & Wiley 2006). The medium diameter DRG neurons (31-40µm) are associated to Aδ-fibers and the small diameter DRG neurons (27-31µm), associated to C-fibers. Both Aδ-fibers and C-fibers transduce noxious nociceptive information (Ramachandra et al. 2013; Hong & Wiley 2006).

1.2 Pain

According to the International Association for the Study of Pain (IASP), "Pain is an unpleasant sensory and emotional experience associated with actual or potential tissue damage, or described in terms of such damage."

Acute pain is essential for an organism's survival, because it recruits protective reflexes to maintain the body integrity and to avoid similar experiences in the future (Lampert et al. 2010). An organism can experience acute pain because DRG and trigeminal neurons convey the sensory stimuli elicited in nociceptors into quantitative information relative to the potential/actual danger situation to the central nervous system (CNS) (Waxman et al. 2000).

1.2.1 Chronic pain syndrome

Chronic pain (CP) syndrome is a limiting condition with physical, psychological and economic consequences to the patients (Azevedo et al. 2012), defined as a pain lasting greater than six months (Cathy & William 1998). The aetiology of CP includes trauma, metabolic or autoimmune disorders, infection, anti-retroviral treatment and chemotherapy (Tsantoulas & McMahon 2014).

Neuropathic pain syndromes are CP disorders descendent from nerve injuries or disease of parts of the nervous system (Baron 2006). Although the onset of neuropathic pain must evolve the nociceptive system, the pain perception persists even in the absence of the causing damage (Campbell & Meyer 2006). Inflammatory pain is initiated by tissue damage or inflammation (Woolf & Mannion 1999) and certain types of persistent inflammatory pain may be seen as an extension of the normal healing process (Theile & Cummins 2011).

The symptoms of CP comprise hyperalgesia (an exaggerated sensation to a painful stimuli) at the site of the injury and surroundings (secondary hyperalgesia), allodynia (pain perception in response to a non-painful stimuli), spontaneous pain,

paresthesia (abnormal sensation) and dysesthesia (unpleasant paresthesia) (Tsantoulas & McMahon 2014; Sun et al. 2012). Moreover, the consequences of CP may lead patients to an increased feeling of anxiousness and depression, reducing their quality of life (Mansour et al. 2014).

As previously said, hyperalgesia in patients with CP may be primary or secondary. Primary hyperalgesia occurs at the site of the injury, being mediated in part by sensitization of primary afferent nociceptors, whereas the secondary hyperalgesia occurs in the uninjured tissue surrounding site of the injury, causing mechanical but not thermal hyperalgesia (Campbell & Meyer 2006).

1.2.2 Mechanisms of neuropathic and inflammatory pain

CP can be of neuropathic or inflammatory origin. Neuropathic pain is caused by a damage or disease within the nervous system, classified as focal or multifocal lesion of the PNS (e.g. post-traumatic neuralgia or phantom limb pain), generalized lesion of the PNS (e.g. painful diabetic neuropathy), lesions in the CNS (e.g. spinal cord injuries or multiple sclerosis) or even complex neuropathic disorders (complex regional pain syndromes type I and II) (Baron 2006). Local inflammatory pain may appear in the absence of nerve trauma, as in the patients with low back pain or postherpetic neuralgias (Wang et al. 2007). Nonetheless, besides the neuropathy, an inflammatory component is also normally associated in the case of tissue damage (Eijkelkamp et al. 2012).

Alterations in pain perception are a consequence of neural plasticity in pain syndromes and may occur from two mechanisms: modulation and modification (Woolf & Salter 2000).

Modulation of neural excitability is a consequence of reversible changes in the excitability of primary afferents and central neurons. The exposure of the terminals from the periphery to sensitizing agents during tissue damage or inflammation may activate terminals. These agents will sensitize terminals to subsequent stimuli, even if

it previous did not activate nociceptors (Woolf & Salter 2000). Sensitizing agents, include inflammatory mediators, amines, prostanoids, kinins, purines, protons, and neurotrophic factors, such as the NGF (Amaya et al. 2006). The threshold of transducer channels is reduced, there is an increase in terminal membrane excitability (Wang et al. 2007). At the same time, intracellular cascades of kinases are also activated, leading to phosphorylation of, for example, Nav1.8 (*see section 0*), altering the threshold of activation, kinetics and magnitude of current transferred after depolarization (Gold et al. 1998).

There are different mechanisms involved in neuropathy and inflammation including those related with such modulation of primary neurons. Target-derived growth factors, are important in neural development and also in the maintenance of its phenotype in adult. In a neuropathic condition, these factors decrease as they may loss contact with the target (cell body), leading to changes in the components of nociception, such as synaptic modulators, ion channels and other proteins. Contrarily, an inflammatory condition leads to an increase in those target-derived growth factors, leading to the upregulation of certain ion channels, such as VGSC (*see section 0),* transducers and also in the neurotransmitters and neuromodelators, namely substance P and brain-derived neurotrophic factor (BDNF) (Woolf & Salter 2000).

When the nerve is partially damage, the expression of VGSC is increased in the affected fibers and the myelinated damaged fibers undergoes a Wallerian degereneration, releasing NFG. The intact fibers from the axon, when in contact with the released NGF, will increase their expression of Na^+ channels, TRPV1 channels and adrenoreceptors, therefore increasing the sensitivity of those uninjured fibers (Baron 2006).

Abnormal sensations in CP are a consequence of sensitized nociceptors and changes in ion channel complexes. Nevertheless a change in the phenotype of A-fibers may also occurresulting, for example, in allodynia.

1.3 Neuroexcitability and voltage-gated ion channels

Before focusing on the cellular mechanisms involved in nociception and pain, particularly those related with neuroexcitability, it is important to take a step-back and introduce some basic and relevant background related to the electrical transmission of signals.

The existence of a semi-impermeable cellular membrane separating the intra from the extracellular fluids and the different composition of these fluids impose to each of their components an electrochemical gradient. The variations in the several electrochemical gradients are useful to signalling and metabolism of cells (Denac, Mevissen & Scholtysik, 2000). Beside adenosine triphosphate (ATP)-consuming pumps and co-transporters cell membranes also have in their composition ion channels, whose function is to allow the passive flow of ions between the inside and the outside of cells. The conformation of ion channels alters between a non-conducting and a conducting state in response to internal or external stimuli (e.g., membrane potential change, a neurotransmitter or other chemical release or mechanical deformation), illustrated in Figure 6 (Hille 2001). The channel's response to the stimuli is called gating and it can be open or closed. Figure 6 illustrates the gating of VCGS.

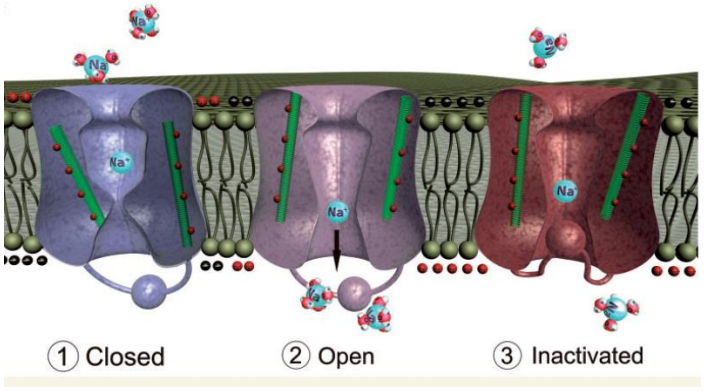

Figure 6 – Gating cycle of VGSC. 1- At rest membrane potential (RMP), the channel has a closed conformation and the passage of ions is blocked from the intracellular side of the membrane. **2-** After a depolarization of the membrane potential, the inner gate opens and the channel assumes an open conformation, allowing the passage of Na^+ according to the electrochemical gradient (in physiological conditions from the extra to the intracellular side of the cell). **3-**The previous inward Na^+ current depolarizes even more the membrane potential and forces the extracellular gate to close and the channel assume an inactive non-conducting conformation. After the repolarization of the membrane potential, the extracellular gate opens and the intracellular closes, consequently the channel assumes the original closed conformation and is ready to be activated. Adapted from Eijkelkamp et al. 2012.

The excitability of neurons and other excitable cells is regulated by voltage gated Na^+, potassium (K^+) and Ca^{2+} channels, leak channels and ligand-gated channels. These channels are able to set the rest membrane potential (RMP), AP initiation, depolarization and repolarization, refractory period between action potentials and neurotransmitter release (Waxman & Zamponi 2014).

Figure 7 illustrates the role of ion channels in nociception. If the receptors in nociceptors are stimulated and the membrane potential is depolarized to a critical threshold potential, an AP is generated. Due to their nature, the impulses can travel rapidly without distortion from the nociceptors to the other end of the axon. Note that the frequency firing of AP obey to a refractory period, in which the channel is recovering from inactivation, and a second AP cannot be generated (Hille 2001).

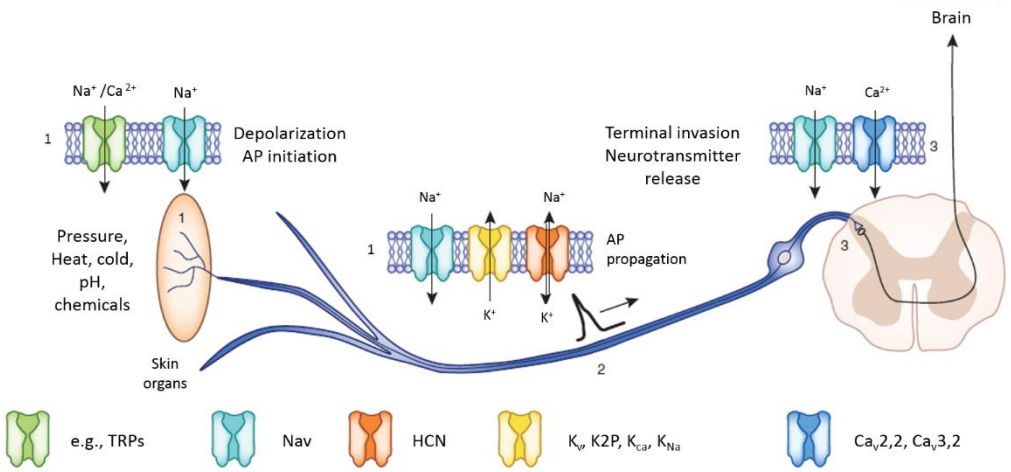

Figure 7 – Propagation of noxious stimuli in the primary afferent pathway. 1- Different stimuli, such as pressure, heat, cold, pH or chemicals can activate nonselective cations (e.g. TRPs) and VGSC (Nav) channels at the free nerve endings of the primary afferents in skin and organs, leading to a depolarization of membrane potential and an AP initiation. **2-** The voltage-gated Na^+ and K^+ channels along the axon are responsible for the AP propagation to the other synaptic terminal at the dorsal horn. **3-** The depolarization induced by VGSC triggers the activation of voltage gated Ca^{2+} channels (Ca_V), allowing the release of neurotransmitters into the synaptic fence. Adapted from Waxman & Zamponi 2014.

Voltage-gated ion channels share some functional features: the aqueous pore is formed by four homologous domains covalently linked in tandem or formed by oligomerization of smaller subunits. These channels have a steeply voltage-dependent gate that open with a delay in response to membrane depolarization, close after its repolarization and inactivates under sustained depolarization (Hille 2001).

Voltage-gated Ca^{2+} channels are relevant to initiation of AP and translation of the electrical signals into chemical signals. At the RMP, low-voltage activated Ca^{2+} channels may open to depolarize the cell, bringing it closer to the firing threshold of Na^{+} spike. At the dendrites and soma, other Ca^{2+} channels (high voltage-activated) became open after the depolarization of RMP, Ca^{2+} flows in and it acts locally as a secondary messenger in many pathways (Waxman & Zamponi 2014).

Voltage-gated K^{+} channels are key determinants of neuronal firing frequency and spike duration (Waxman & Zamponi 2014). Much more diverse than Na^{+} and Ca^{2+} channels, among other functions, K^{+} channels stabilizes the RMP, bringing it closer to the hyperpolarized K^{+} electrochemical gradient and far from the depolarized firing threshold. In an open conformation voltage-gated K^{+} channels allow the appearance of an outward K^{+} current across the cell membrane that counteracts the inward current of Na^{+} and Ca^{2+}, limiting the neuronal excitability. In sensory neurons, voltage gated K^{+} channels inhibit peripheral excitability by counteracting AP initiation at peripheral nerve terminals (Waxman & Zamponi 2014; Tsantoulas & McMahon 2014; Hille 2001).

1.3.1 Voltage-gated Sodium channels (VGSC)

VGSC are indispensable for AP generation. Its ability to change from a closed to an opened conformation in response to a depolarization of the membrane potential within milliseconds, produces a fast inward Na^+ current in excitable cells, allowing the rising phase and propagation of AP to occur. The inward Na^+ current drives the membrane potential to even more depolarized potentials and consequently the channel changes to an inactivated non-conducting state, leading to a decay in the Na^+ current. After a refractory period wherein the membrane is repolarized, the channel returns to the rest conformation (closed) and is ready to be again activated. The conformation cycle of VGSC allows repetitive firing of AP (Yu & Catterall 2003; Wang et al. 2011).

In mammal cells, nine isoforms of the VGSC were identified, from Nav1.1 to Nav1.9, distributed differentially through the excitable cells. Nav1.1, Nav1.2, Nav1.3 and Nav1.6 are mainly expressed in the CNS, while Nav1.7, Nav1.8 and Nav1.9 are mainly present in the PNS; and finally, Nav1.4 and Nav1.5 are expressed in adult skeletal muscle and heart muscle, respectively (Catterall et al. 2005).

VGSC are also classified according to their sensitivity to tetrodotoxin (TTX), a natural toxin that blocks VGSC. Hence, there are TTX-sensitive VGSC (Nav1.1, Nav1.2, Nav1.3, Nav1.4, Nav1.6 and Nav1.7) blocked with nanomolar concentrations of TTX; and TTX-resistant Na^+ channels (Nav1.5, Nav1.8 and Nav1.9) blocked only at milimolar concentrations of TTX (Gilchrist et al. 2014).

VGSC is a multimeric glycoprotein complex (260-280kDa) formed by one α-subunit associated to one or more auxiliary β-subunits (Yu & Catterall 2003). The pore forming α-subunit has the functional characteristics of the whole channel, whereas the β-subunit has a more regulatory function of trafficking, gating properties and kinetics of the endogenous VGSC (Denac et al. 2000; Ho et al. 2012).

1.3.1.1 α-Subunit

The α-subunit of VGSC (Nav1.1 to Nav1.9) is composed by four homologous domains (DI-DIV) that form the ion-conducting pore (Noda et al. 1984). Figure 8 illustrates the structure of the α-subunit, showing that each domain is formed by six transmembrane segments (S1-S6) connected by three interdomain loops at the cytoplasmic surface, intersegment loops and an additional pore loop located between the S5 and S6 segments at the extracellular side of the membrane. The later pore loop narrows the entry of the channel from the exterior side, limiting the size of the conducted ions and partially contributing to the ion selectivity of the channel. The S5 and S6 segments form the inner side of the pore, also contribute to the ion selectivity of the channel and provide a bigger exit from it (Catterall et al. 2005; Habib et al. 2015).

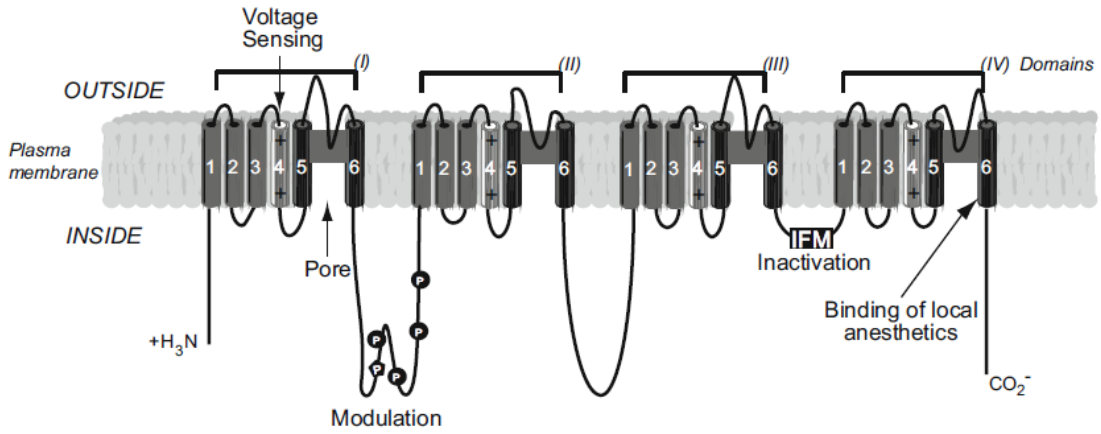

Figure 8 – Primary structure of the α-subunit of VGSC. The α-subunit is an integral membrane protein, formed by four homologous domains (DI-DIV), connected by interdomain loops (solid lines) at the cytoplasmic side of the membrane. Each domain is composed by six transmembranar segments (S1 to S6; grey cylinders), connected by nonconserved hydrophilic sequences (solid lines). The highly positively charged S4 segment constitutes the voltage sensor of the channel, while S5 and S6 segments forms the selectivity pore. The function of the channel may be modulated by phosphorylation at the interdomain sequence connecting D-I and D-II; and the interdomain loop between the D-III and D-IV have the inactivation gate of the channel. The inner pore residues from the S6 segments of the domains I, III and IV are the binding site of some anaesthetics drugs. Reproduced from Habib et al. 2015.

At membrane rest potential, the many positives charges from S4 are attracted and stabilized by the negative charges from the neighbouring S1, S2 and/or S3 segments, conferring to the VGSC a closed conformation. When the cell membrane is depolarized, the former electrostatic forces are relieved and the S4 segments move outwards, rotating and the gate assumes an open conformation. This activation of the channel allows the passive flow of Na^+, causing an increase in the Na^+ inward current. After a sustained depolarization of the membrane, the inactivation gate formed by the intracellular loop connecting the domains III to IV blocks the channel from the inner side membrane, leading to downstroke of the AP (Catterall 2010; Catterall et al. 2005).

1.3.1.2 β-subunits

Four subunits of the β-subunit of VGSC are identified to date (β1, its spliced variant β1B and β2 to β4) (Brackenbury & Isom 2011). Excepting the β1B-subunit, the remaining β-subunits share a similar type I membrane topology: a single membrane-spanning α-helix, a short intracellular C-terminus and a large extracellular N-terminus incorporating an immunoglobulin-like fold. β2 and β4-subunits are disulfide linked to VGSC α-subunit whereas β1 and β3-subunitis are associated non-covalently (Brackenbury & Isom 2011; Ho et al. 2012).

β-subunits affects the insertion of the VGSC in the cell membrane, also it regulates the gating, voltage-dependence and kinetics of the α-subunit of VGSC. However, those effects are cell specific and the existence of conflicting results related to the influence of β-subunits upon α-subunits of VGSC difficults the attribution of specific functions to it. Moreover, besides modulation of the excitability of Na^+ channels, β-subunits are also members of the immunoglobulin superfamily of cell adhesion molecules and regulate cell adhesion and migration (Brackenbury & Isom 2011).

β3-subunit have 50% homology with β1-subunit and exhibits a complementary distribution in the rat brain, DRG neurons and spinal cord. In DRG neurons, β1-subunit mRNA is mostly expressed in the large Aβ-fibers while β3-subunit mRNA is highly expressed in small C-fibers with lower levels present in Aδ-fibers. In the dorsal horn, the β1-subunit mRNA was detected in all laminae and the β3-subunit mRNA was expressed exclusively in the laminae I/II and X (Shah et al. 2001; Shah et al. 2000).

An increase of β3-subunit transcripts is associated to neuropathic syndromes (*see section 1.2.1)*, such as nerve injury and painful diabetic neuropathy (Shah et al. 2000; Shah et al. 2001). Moreover, while some have reported the absence of β2-subunits in cultured DRG neurons (Shah et al. 2000), others have reported that *in vivo*, β2-subunits regulated the TTX-sensitive Na^+ channels electrophysiological properties and expression in small DRG neurons, modulating the response to pain in mice (Lopez-Santiago et al. 2006).

The apparent conflicting results from the literature indicate a possible influence of β-subunits in pain conditions, although the real effect need further research.

1.3.1.3 Sodium channels and pain pathways

The different patterns of VGSC isoforms expression confers different electrical characteristics to excitable cells. The outcome of electrogenesis is a product of the activity of the entire population of channels present at the cellular membrane. As mentionedabove,Nav1.7, Nav1.8 and Nav1.9 are predominantly expressed in peripheral neurons (Rush et al. 2007; Dib-Hajj et al. 2012). The VGSC are produced in the soma of the DRG neurons and transported to their peripheral targets by axoplasmic mechanisms(Coward et al. 2000).

Table 2 summarizes the principal features from the VGSC expressed in DRG neurons and their roles in electrogenesis (Rush et al. 2007).

Nav1.7 is preferentially expressed in peripheral neurons, in all DRG neurons. It is also present in sympathetic ganglion neurons, myenteric neurons, olfactory sensory neurons, visceral sensory neurons and smooth myocytes (Dib-Hajj et al. 2012).

Table 2 – Principal features from VGSC expressed in DRG neurons. Adapted from Rush et al. 2007.

VGSC	Distribution	Biophysical characteristics	Action potential
Nav1.7	All DRG neurons	• Rapid activation and inactivation • Slow recovery from inactivation • Slow closed state inactivation	• Amplifies subthreshold stimuli
Nav1.8	Small and medium DRG neurons	• Very depolarized Activation/Inactivation • Rapid Recovery from inactivation	• Major contributor in AP upstroke • Repetitive firing in small neurons
Nav1.9	Most small $IB4^+$ small DRG neurons	• Hyperpolarized activation • Overlapping activation and inactivation • Ultra-slow inactivation	• Setting RMP • Amplification of small inputs and/or • Maintaining activation of Nav1.8
Nav1.3	Misexpressed in CP	• Rapid Repriming • Ramp current • Persistent current	• Ectopic firing

Biophysically, Nav1.7 presents a fast activating and inactivating Na^+ current (Klugbauer et al. 1995), with a slow recovery from inactivation and displays a slow closed-state inactivation that consequently allows the channel to produce a substantial ramp current that amplifies small depolarizing inputs (Cummins et al. 1998). The slow recovery from inactivation from this channel impairs it to support high frequency repetitive firing (Dib-Hajj et al. 2012).

A link is established between mutations in the Scn9A gene, coding for the Nav1.7 protein, and pain related diseases. A recessive Scn9A loss-of-function mutation leads to congenital insensitivity to pain (CIP), where acute thermal and mechanical insults are not perceived by such patients (Cox et al. 2006). A dominant Scn9A gain-of-function mutation is described in two painful syndromes, namely erythromelalgia (IEM) and paroxysmal extreme pain disorder (PEPD) (Brouwer et al. 2014). Furthermore, Nav1.7 has been associated with inflammatory and neuropathic pain syndromes (Black et al. 2004).

The TTX-resistant channel Nav1.8 is expressed mainly in the DRG neurons and their axons and in trigeminal and nodose ganglion neurons from the PNS (Akopian et al. 1996; Waxman & Zamponi 2014).

Nav1.8 displays a depolarized voltage dependence of activation and inactivation, a slowly inactivating Na^+ current (Akopian et al. 1996) and a rapid recovery from inactivation (Blair & Bean 2003). In fact, Nav1.8 produce the majority of inward Na^+ current during the AP upstroke in DRG neurons and enables repetitive firing (Renganathan et al. 2011). Gain-of-function mutations in the Scn10 gene, coding for Nav1.8 protein, may produce hyperexcitability and inappropriate spontaneous firing in DRG neurons in about 5% of patients with painful peripheral neuropathy who do not carry Nav1.7 mutations (Waxman & Zamponi 2014). Nav1.8 has been also associated with inflammatory and neuropathic pain syndromes (Wood et al. 2004; Coward et al. 2000).

The TTX-resistant channel Nav1.9 produces a large persistent current that is slowly activated at hyperpolarized potentials, close to the RMP. Its voltage dependence of steady-state inactivation is intermediate comparing to Nav1.7 and Nav1.8 currents. The overlap between activation and inactivation gives the persistent appearance to Nav1.9 Na^+ currents, that prolongs and enhances small depolarizations and consequently increases excitability of DRG neurons (Dib-Hajj et al. 2002; Waxman & Zamponi 2014).

In physiological conditions, the TTX-sensitive channel Nav1.3, is expressed in CNS neurons and in developing sensory neurons from PNS (Wood et al. 2004). However, in adult DRG neurons following inflammation or nerve injury it may become upregulated. (Black et al. 2004). Nav1.3 produces a persistent current and responds to small depolarizations close to the RMP, leading to amplification of small inputs. It also recovers rapidly from inactivation and therefore supports repetitive firing (Waxman & Zamponi 2014).

1.4 Current approaches to study Chronic pain

1.4.1 Animal models of Chronic pain

Much of the study related to the physiopathology of CP relies on animal pain models, resulting in nociceptive sensitization similar to the key components of CP syndrome experienced in humans (Descalzi et al. 2015). Among all laboratory animals, rats are the elected. However, the use of mice is also generalized, due to the possibility of production of transgenic lines. However, the use of mice is not profitable in studying pain associated to polygenic clinical conditions like back pain, osteoarthritis or fibromyalgia (Mogil 2009). The use of rodents to study CP is a well-accepted strategy because drugs that shown some efficacy in CP patients have demonstrated activity in animal models of pain (e.g., gabapentin/pregabalin) (Liu & Wood 2011; Coward et al. 2000).

Animals may not self-report pain, but their behaviour to noxious stimuli can still be quantified. Typical behaviour responses assessed in pain studies are reflexes or innate responses (e.g. paw withdraw, linking the sensitized zone, tail flick) and do not evolve the higher circuits of pain perception (Mogil 2009).

The perception of pain is subjective due to many factors and, in humans, for example, females are more sensitive to pain than males (Bartley & Fillingim 2013). Besides, not all individuals that are subjected to a disease or trauma develops CP. Therefore, when studying CP, individual variation should be taken in account. Moreover, in acute assays, female rats and mice are more sensitive than males and males respond better to analgesic drugs (Mogil 2009).

1.4.1.1 Inflammatory pain models

Since CP may have different aetiologies, pain research relies in several models according to it. In inflammatory pain models it is common to use immune system-activating substances (e.g. complete Freund's adjuvant (CFA) or carrageenan), nociceptor-sensitizing molecules (e.g. bradykinin, pro-inflammatory cytokines, prostaglandins, serotonin or substance P) or substances that act on specific structures of PNS (e.g. formalin or capsaicin) (Yu et al. 2011). In monoarthritis assays, the injection of the immune system-activating substances, such as CFA in the knee or hind paw is frequent (Mogil 2009). The behavioural effects of the previous pain model are long-lasting, including mechanical and heat, but not cold hyperalgesia and allodynia (Sandku 2009).

Previous studies in inflammatory pain show an increase in VGSC expression in correspondent DRG (as referred to in *section 1.3.1.3*), more particularly an increase in Nav1.3 and Nav1.6-Nav1.9 (Black et al. 2004).

1.4.1.2 Neuropathic pain models

As mentioned before, peripheral nerve injuries may result in the development of CP (Hains et al. 2004). In neuropathic pain syndromes, partial damage to nerves are more common than nerve transections (only observed in axotomies). Partial nerve damage may be due to cuts, stretching, compression or neuritis, and therefore, most neuropathic pain models rely on a surgical approach (Mogil 2009).

For instance, in the chronic constriction injury (CCI) model, one of the most commonly used models to study neuropathic pain in rodents and, represented in Figure 9, four loose ligations are tied around in the sciatic nerve, inducing hyperalgesia, cold and mechanical allodynia (Bennett & Xie 1988). The resulting constriction does not stop the blood flow and produces an inflammation, leading to the physiological changes inhered to chronic neuropathic pain (Kajander et al. 1996).

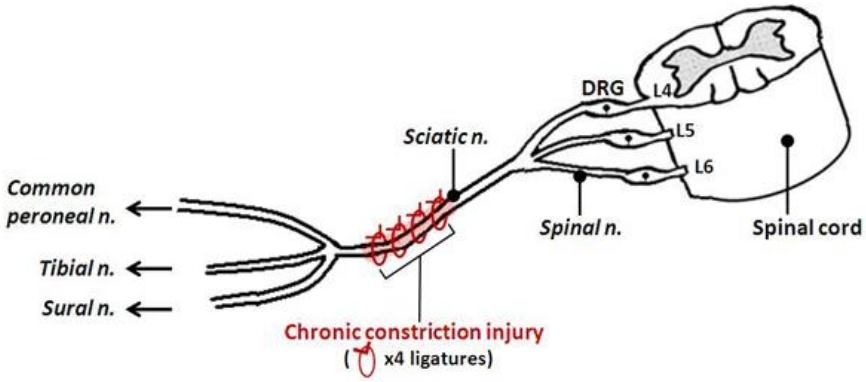

Figure 9 – Chronic constriction injury (CCI) of the sciatic nerve. In the neuropathic CCI model, four loose ligations are performed around the sciatic nerve of rats, before the sciatic notch. The model leads to an inflammatory response against the suture material and a neuropathy resultant from the damage elicited to part of the nerve fibers. Adapted from Austin et al. 2012.

As in axotomies, peripheral partial insults in nerve tissues may lead to the arising of an abnormal mass at the site of injury, called neuroma. Although not all neuromas are painful, some may present spontaneous activity and ectopic sensitivity to thermal, mechanical and chemical stimuli (Campbell & Meyer 2006; Bird et al. 2013). Neuromas express unusual ion channels in their membranes, the accumulation of Nav1.3, Nav1.7 and Nav1.8 (as referred to in *section 1.3.1.3*), has been reported by previous studies (Black et al. 1999; Wang et al. 2011).

1.4.2 Study of the physiopathology of Chronic pain

1.4.2.1 Animal behaviour

Animal behavioural studies have a special relevance in the study of pain. Besides the inducted pain, other factors may influence animal behaviour: grooming, the experimenter identity, animal handling, testing order and environmental factors. Therefore, all behavioural measurements must be strict (Minett et al. 2014).

Non-evoked readouts (e.g. weight bearing or rearings in open field) for the assessment of pain are interesting observations to perform in pain studies. In weight bearing assays, the body weight distribution between ipsilateral (injured) and contralateral (uninjured) legs of rodents is assessed with a special equipment, being expected to obtain a lower distribution weight in the ipsilateral leg, especially in unilateral inflammatory pain models (e.g. knee monoarthritis). The assessment of the number of rearings that rodents perform in the open field of the behavioural cage is also commonly performed in pain studies (Bagriyanik et al. 2014). When counting number of rearings, it is assumed that a reduction in the number of rear ups is a sign of spontaneous pain in rats (Rutten et al. 2014).

Non-innate evoked responses are the most used read-out in pain studies and reflex behaviour such as paw withdrawal or tail flick in response to noxious stimulation. However, the cerebral cortical structures involved in pain conscious perception may not be involved in the mentioned reflex behaviour (Lascelles & Flecknell 2010).

Paw withdrawal responses are normally assessed in an elevated behavioural cage, with a mesh floor. Mechanical, chemical or radiant stimuli can therefore be applied to the rat's paw via the mesh on the bottom of the behavioural cage. (Austin et al. 2012)

Mechanical allodynia and hypersensitivity can be evaluated using calibrated von Frey monofilaments (vFF) by measuring the number of withdrawal responses from rats as illustrated in Figure 10. The acute stimulation with the filament in the glabrous surface of the hind paw in spaced repetitive presentations gives a reliable measure of the sensitivity of the animal and allows pain quantification (De Sousa et al. 2014).

The secondary hyperalgesia resultant, for example, from monoarthritis of the knee, can also be measured by performing the mechanical assays with the vFF in the glabrous surface of the hind paw.

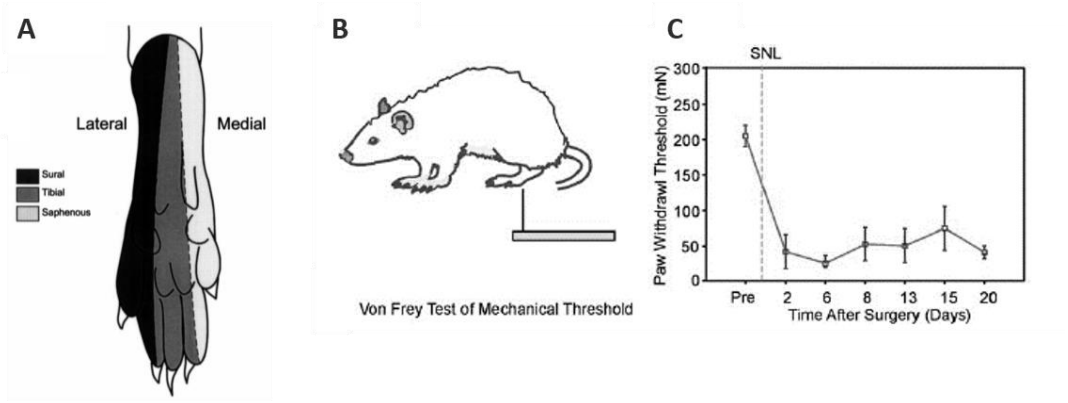

Figure 10 – Measurements of mechanical sensibility on the hind paw from rats. A- The sciatic nerve is bifurcated in three nerves (sural, tibial and common peroneal nerve) each of the branches enervates different areas from the leg and paw of rats, together with the saphenous nerve. The plantar surface of rats hind paw is enervated by the sural, tibial and saphenous nerves; an overlap of the nerve fibers may occur in the boundaries of the three areas delimited in the figure. Adapted from Decosterd & Woolf 2000. **B**- Mechanical allodynia and hypersensitivity may be assessed by stimulation of the glabrous surface of hind paws of rats with calibrated von Frey filaments and observing the withdrawals evoked. **C**- The alterations in paw withdrawal thresholds can be measured during the time of progression of the pain model. The figure illustrates an increase in the sensibility of rats, resulting from the neuropathic spared nerve ligation (SNL) pain model, where a constriction is applied in the descendent root from the L5 dorsal root ganglia. Adapted from Campbell & Meyer 2006.

Thermal allodynia is also a consequence of CP and heat sensitivity can be measured subjecting rodents to a radiant heat source under the glabrous surface of the paws (Fan et al. 2011). Cold allodynia may also be assessed by applying acetone into the surface of the hind paw (Amin & Hosseinzadeh 2012).

1.4.2.2 Electrophysiology

As mentioned before, biological membranes of excitable cells have in their surface numerous ion channels, such as voltage-dependent or ligand-activating channels. The ion currents recorded from an excitable cell are the result of the overall net flux ionic currents resulting from the activity of those ion channels present at the cell membrane (Rush et al. 2007).

In patch-clamp electrophysiology experiments, namely in the whole-cell voltage-clamp configuration, the experimenter controls the voltage potential across the cell membrane. Thus, by keeping the membrane potential at a desired value, one can

record the ionic currents that flow across the membrane in response to the new membrane potential (Walz et al. 2002).

As mentioned above, in certain diseases, changes in the properties of ionic channels lead to abnormal electric properties in biological membranes, and therefore the study of the ionic currents can provide valuable information to new therapeutic strategies. The presented dissertation aims to study the important biophysical features of ion channels such as the voltage dependence of activation, the current density that flows across the membrane, the kinetics of activation and inactivation of ion channels as well as their dependence of steady-state inactivation and their time of recovery from inactivation.

1.4.2.3 Ion channels expression

The ionic currents measured in electrophysiology studies reflect not only the amount of ion channels present at the cell membrane, but also their conductive properties. The use of biochemical techniques, such as immunohistochemistry and Western blot, allows to correlate the current measured with the amount of ion channels expressed and stored in the cell.

1.5 Current therapies for Chronic pain treatment

It is estimated that one out of five people worldwide suffer from moderate or severe CP and although its high prevalence nowadays, there is no adequate treatment for most type of patients (Theile & Cummins 2011). Current pharmacological therapeutic approaches include non-steroidal anti-inflammatory agents, opioids, anticonvulsants and antidepressants, which may be associated to adverse dose-limiting side-effects, dependence, pharmacological habituation or even loss of pain control (Tsantoulas & McMahon 2014; Iyer & Tanenberg 2013).

Neuromodulation is also an alternative treatment option for CP, it is relatively safe and a possibly effective treatment option for patients (Krames 2014). With this approach a device is inserted into the patient's body and it is programmed to modulate electrically the function of neurons from, for example, the DRG or spinal cord. Nevertheless, neuromodulation treatment has not been found as an effective long-term solution in approximately 50% of patients that had a successful temporary trial stimulation. Moreover, neuromodulation faces other challenges such as the positional or postural effects of patients and the device programming to address individual's pain (Liem et al. 2013).

The lack of viable treatment options to some CP patients and the existence of important side-effects associated with some of the current therapies creates a huge need for better and smarter drugs targeting the underlying neurobiological mechanisms that produce pain. DRG neurons have been pointed as a possible pharmacological target to modulate CP due to its peripheral location. Moreover, Na^+ channels, due to its essential function on initiation and transmission of AP have also been studied in this context (Pope et al. 2013; Dib-Hajj et al. 2009). Accordingly, and as referred to above, it has been shown that certain VGSC currents are dysregulated in DRG neurons following nerve injury and gain-of-function mutations in Nav1.7 or Nav1.8 channels lead to severe pain syndromes (*see section 1.2.1.3*). This is also of particular importance when considering a novel pharmacological treatment of pain

involving effective drugs blocking VGSC and that do not need to cross the blood-brain-barrier (i.e., acting locally at DRG level and blocking the abnormal brain perception of pain), avoiding CNS side-effects.

2. Objectives

The study of the pathophysiological mechanisms and structures underlying CP is essential to unveil new therapeutic approaches to treat this erosive disease. In this regard, VGSC have the ability to initiate the electrical signalling in excitable cells, a characteristic that makes them potential drug targets, along with its preferential localization (namely the isoforms Nav1.7, Nav1.8 and Nav1.9) on DRG neurons. Nevertheless, there is still a great demand for novel functional studies of those currents/channels sub-types specifically involved in the processes of CP, namely in neuropathic and inflammatory pain.

Therefore, the overall goal of the present dissertation was to study alterations in VGSC currents/channels in DRG neurons from rat models of neuropathic (CCI of the sciatic nerve) and inflammatory (CFA-induced monoarthritis) CP, further validating DRG neurons as a pharmacological target to the treatment of CP.

More specifically, this study aimed to:

- identify the biophysical and pharmacologic patterns that are altered following induced CP, by the study of Na^+ currents in small DRG neurons (derived from CFA, CCI and control rats) trough whole-cell voltage-clamp technique;

- study the VGSC expression, namely the expression of Nav1.7 and Nav1.8 isoforms, in DRG neurons derived from CFA inflammatory and CCI neuropathic rat models through immunohistochemistry and Western blot techniques; and

- correlate those findings with animal behaviour tests, specifically with the detection of mechanical hyperalgesia and cold allodynia.

Overall, results showed a development of hyperalgesia and an abnormal function and expression of VGSC in DRG neurons following inflammatory and neuropathic pain in rat models, contributing to the validation of VGSC in DRG neurons as potential targets for novel analgesics.

3. Methods

Animal experiments with young adult Wistar rats were performed at the rodent facility of NOVA Medical School/Faculdade de Ciências Médicas (NMS|FCM), in accordance with its Ethical Committee and with 86/609/EEC Directive for animal care and experimentation. Animals were purchased from NMS|FCM and caged in a 12h light/dark cycle, at room temperature (21 ± 3°C) with water and food *ad libitum*. They were divided in four different groups: 1) complete Freund's adjuvant (CFA) and respective 2) naïve control, 3) chronic constriction injury (CCI) and respective 4) sham control, as described below (*see section 3.1*).

After establishment of those animal pain models, the onset of mechanical hyperalgesia and the development of cold allodynia was studied. Consequently animals were sacrificed for consequent harvesting of DRG ganglia. The biophysical properties of Na^+ currents were studied by whole-cell voltage-clamp in dissociated DRG neurons and protein expression of VGSC in DRG ganglia was assessed by immunohistochemistry and Western blot techniques (Figure 11).

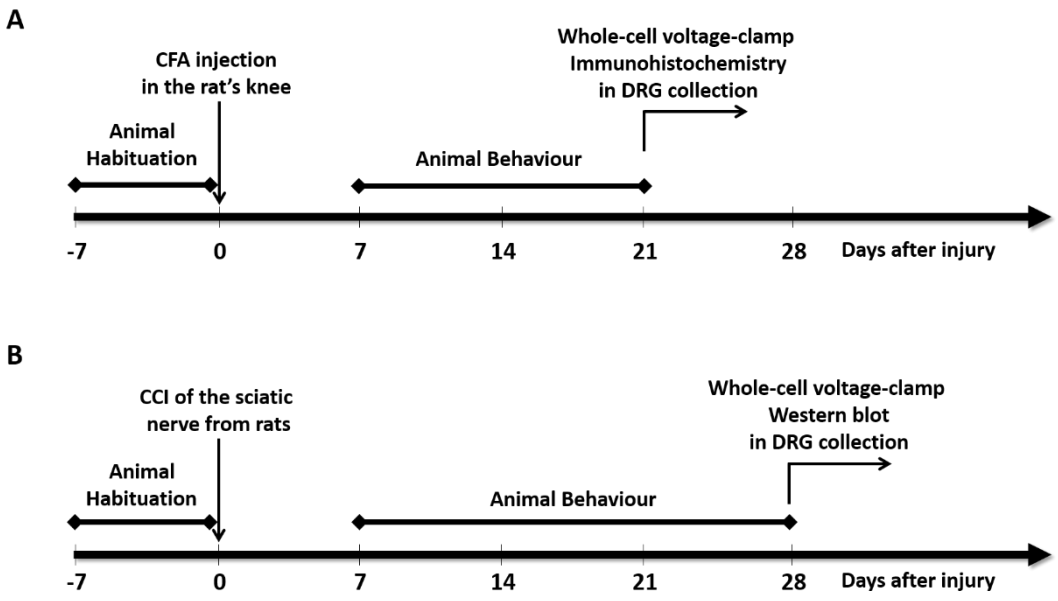

Figure 11 – Experimental design from the inflammatory (A) and neuropathic (B) pain models. For this experiments, both injured and control rats had a week of habituation to the equipment and operator from the animal behaviour experiments. **(A)** For the CFA pain model, animals were subjected to pain behaviour tests at the 7th, 14th and 21st days after injury, while for **(B)** CCI pain model, it was prolonged until the 28th day after injury. At the end of the course of the experiments, the DRG neurons from CFA **(A)** were harvest for whole-cell voltage-clamp and immunohistochemistry, while the DRG neurons from CCI **(B)** were harvest for whole-cell voltage-clamp and Western blot analysis.

3.1 Animal Pain Models

3.1.1 Inflammatory Pain Model: Complete Freund's adjuvant (CFA) – induced monoarthritis

Seven male Wistar rats (initial weight 120-170g) were deeply anesthetized with ketamine/diazepam (100/5 mg/kg i.p.) prior to the injection of 100 µL of complete Freund's adjuvant (CFA, Sigma F5881) into the right knee joint (ipsilateral) with at least 50 times of gently rubbing in a circular manner. Five naïve rats were used as controls: the only procedure performed with this rats was using anaesthesia as the CFA ones; no other injection was applied, as any injection on the knee joint may induce inflammation by itself. Knees' perimeters were measured in all rats to assess the development of swelling as a consequence of the inflammation caused by CFA (data not shown). This procedure was performed together with the researcher from the laboratory, Marisa Sousa (PhD).

All the animals were let to recovery after anaesthesia, one per cage, as in the course of the experiment.

3.1.2 Neuropathic Pain Model: Chronic constriction injury (CCI) of the Sciatic Nerve

Thirteen female Wistar rats (130g-170g) were deeply anesthetized with ketamine/diazepam (100/5 mg/kg i.p.). The injury was performed as previously described (Bennett & Xie 1988) with collaboration of the plastic Surgeon (Maria Angélica Roberto (MD), Centro Hospitalar de Lisboa Central EPE).

The sciatic nerve of the right (ipsilateral) leg was accessed by the exposure of the mid-tight muscles by a blunt dissection with an iris scissor at the fascial planes. For a better access of the nerve, retractors were used. Four chromic gut (4.0, Catgut Chrom®) loose ligations were tied at the mid-thigh of the nerve, as shown on Figure 12. For the eight sham control rats, the procedure consisted in the exposure of the same section of the sciatic nerve from the right (ipsilateral) leg. Suture of muscle was

performed with absorbable polyglycolic acid (5.0, Safil®) and suture of skin with soft silk (6.0, Silkam®) in both CCI and sham animals.

Figure 12 - Chronic constriction of the sciatic nerve from a rat included in this study. The procedure was performed as previously described by Bennet & Xie (Bennett & Xie 1988).

All the animals were let to recovery after anaesthesia one per cage. During the 28 days of development of the model, they were housed two littermates per cage, one CCI with one sham.

3.2 Animal behaviour

Animals were let one week for habituation with the equipment and operator prior to the establishment of the pain models. The operator was blind for each group of rats. A baseline for mechanical sensitive was obtained in the last two days of the habituation week. Behaviour tests were performed between 2 and 7 p.m. at the same weekday, for the entire course of establishment of the pain models.

3.2.1 Spontaneous pain

During the first two minutes of habituation, before the mechanical hyperalgesia testing, the number of vertical rearings in the open field of the behavioural cage was quantified, which consists in the number of rear ups that rats performed.

3.2.2 Mechanical sensibility

In order to assess mechanical sensibility in rats, the hind paw withdrawal thresholds were observed using calibrated von Frey monofilaments (vFF) (Bio-VF-M, Bioseb®). Briefly, animals were let to habituation 15 to 20 minutes in the behavioural cage, until cage exploration and grooming activities ceased (Chaplan et al. 1994). Next, the medial plantar surface of both contralateral and ipsilateral hind paws were stimulated by individual vFF with an increasing bending force (0.6, 4, 10 and 15g), according to their sensibility at the habituation week. Each monofilament was presented 5 times for a maximum period of 5 seconds or until a withdrawal response was observed, with at least 5 seconds of interval between measurements (Hulse et al. 2011).

The withdrawal threshold was the filament with the weakest force (g) that gave at least 3 withdrawal responses in the 5 presentations of the filament (Hori et al. 2013).

3.2.3 Thermal sensibility

The development of cold allodynia was observed with the application of an acetone drop with a syringe to the plantar surface of the hind paw, through the mesh floor of the behavioural cage, without touching the paw with the syringe. Measurements were performed for 3 times and any reaction including licking, shacking or rubbing was considered as positive response. The reaction to acetone test was calculated on the basis of frequency of withdrawals, as reported before by Amin and Hosseinzadeh (2012) (Amin & Hosseinzadeh 2012). The frequency of withdrawals is given by the number of trials accompanied by brisk hind paw withdrawal, over the number of total trials, in percentage (Amin & Hosseinzadeh 2012).

3.3 Electrophysiology

3.3.1 Acutely isolated DRG neurons preparation

Rats were overdosed with sodium pentobarbital (100 mg/kg i.p.), followed by decapitation. The DRG harvesting procedure was performed similarly to the described by Malin *et al* (Malin et al. 2007).

Briefly, rats were displaced in a prone position for a better access to DRG neurons. Skin was separated from muscles prior to the exposure of the backbone. With a Littauer bone cutting forceps, a transversal cut was performed in the backbone at the lumbar L1 level. The spinal cord was exposed by cutting with the tip of the Littauer bone cutting forceps, one vertebra at the time, from one side of the vertebra canal to the other.

The spinal cord and dura mater were pulled away from the inside of the backbone gently with the tweezers and the roots of the DRGs became visible. The delicate dorsal root was grasped with a tweezer and by pulling it, booth roots of the DRG ganglia become accessible for the spring scissor to cut it and remove from the vertebra canal. The DRG ganglia from L4 to L6 were removed one at the time and separated in right and left side.

Harvested DRG ganglia were dissected out and placed in cold Krebs dissociation solution consisting of (in mM): NaCl 120, KCl 5, PIPES 20, $CaCl_2$ 1, $MgCl_2$ 1 and glucose 25 saturated with oxygen (pH 7.4, NaOH). Soon after, ganglia were trimmed in three pieces and incubated for45 minutes at 32°C in collagenase 3 $mg \cdot mL^{-1}$ (type IA, Sigma C9891) prepared in Krebs dissociation solution. At 20 minutes of digestion, the pieces of DRG ganglia were mechanically dissociated with a fire-polished Pasteur pipette and at 45 minutes, they were again mechanically dissociated with a smaller diameter fire-polished Pasteur pipette.

Trypsin was added to the previous solution to a final concentration of 2.5 $mg \cdot mL^{-1}$ (Sigma T9201) and digestion was prolonged for more 40 minutes. After digestion, an additional mechanical trituration was performed with an even smaller diameter fire-polished Pasteur pipette; 1.5 mL of Krebs dissociation solution was added to the cell suspension; and cell suspension was centrifuged for 5 minutes at 2000 rpm at room

temperature. The supernatant was discarded and the cell pellet re-suspended in 2mL of Krebs dissociation solution.

Dissociated DRG neurons were plated in poly-L-lysine coated p35 plates (Sarstedt®) prior to whole-cell voltage-clamp experiments. All recordings were performed within 8 hours of dissociation.

3.3.2 Whole-cell voltage-clamp

Small DRG neurons (10 -25 µM) were visually selected by size with a graduate ocular for whole-cell voltage-clamp recordings. Voltage-activated Na^+ currents were recorded with an Axopatch 1D amplifier (Axon Instruments®) and stored using a DigiData 1200 interface (AxonInstruments®) and pCLAMP 5 software (Axon Instruments®) at room temperature.

Microelectrodes (2-3MΩ) were pulled from borosilicate glass (Science Products GmbH®, GB150T-8P) and filled with an internal solution containing (in mM): NaCl 10, CsF 140, HEPES 10 and EGTA 5 (pH 7.2, CsOH). During recordings cells were kept under continuous perfusion by gravity in a bath external solution containing (in mM): NaCl 100, KCl 5, HEPES 10, $CaCl_2$ 1.8, $MgCl_2$ 1, TEA-Cl 30, $CoCl_2$ 2, 4-amino-pyridine 3, glucose 25 (pH 7.4, NaOH) (Costa 1996).

After the contact between the tip of micropipette and cell membrane surface, a continuous negative pressure was applied until a high resistant seal was formed. Whole-cell access was achieved by applying a more negative but still gently pressure to rupture the cell membrane. A holding potential of -70mV was set and transients were immediately set to zero, series resistance was compensated about 75-80% as necessary. The value of whole-cell capacitance (Cm) was obtained directly from the amplifier after transient compensations. Recordings were performed with a low pass filter with a cut-off frequency of 10kHz, with a sampling rate to record Na+ currents with a minimum frequency of 20kHz. The liquid junction potential for the used solutions was 9.3 mV and data were not corrected to this value. Leak subtraction was performed online by P/4 subtraction on pCLAMP 5 software (Axon Instruments®).

Voltage protocols were performed 5 minutes after establishment of whole-cell configuration to allow dialysis of the internal solution into the patched cell.

Total Na^+ current was elicited by the activation protocol, where from a holding potential of -70mV, to a pre-pulse of 60ms at -110mV for total removal of inactivation of Na^+ channels, cells were subjected to test pulses of 50ms from -50 to +10 mV in a 10 mV increment.

The voltage dependence of steady-state inactivation was also studied: from the holding potential of -70mV, a pre-pulse is elicited to the voltage at which one intents infer about the voltage dependence of inactivation, followed by the command pulse to a voltage where full activation is obtained (+10mV). In this experiment, series of pre-pulses ranging from -120 to 0mV were tested.

To study the recovery from inactivation of VGSC, the following protocol was used: from the holding potential cells were pulsed to -110mV to achieve full removal of inactivation, followed by a short pulse to 0mV to inactivate the VGSC. The test pulses were elicited from -110mV to 0mV at different times after the first pulse to 0mV, the delays varied from 0 to 3500ms.

The electrophysiology data was analysed with a combination of the software Clampfit 10.3 (Axon Instruments®), Microsoft Excel (Microsoft Office 2013 Professional Plus®), Origin Pro 8 (Microcal Software®) and NFit (Texas University®).

The voltage dependence of conductance of Na^+ currents was studied by transforming the peak currents from the potentials studied in the activation protocol in conductance values, using the Equation 1:

$$G = I/(E_{Na^+} - Vm\,) \qquad \textit{Equation 1}$$

where G is the conductance, I current amplitude, E_{Na^+} is the reversal potential of Na^+ estimated from the extrapolation of the rising phase of the current-voltages (I-V) relationship curves for each cell and Vm is voltage of the pulse command (Ribeiro & Costa 2000).

The Na^+ conductance values were normalized for the maximal response (G/G_{max}) and plotted against step command potential. The resulting curve had the shape of a Boltzmann curve with the Equation 2:

$$G/G_{max} = (A_1 - A_2)/\{1 + \exp[(Vm - V_H)/V_S]\} + A_2 \qquad \textit{Equation 2}$$

where V_H is the half-activation potential, Vs is the slope constant, A_1 and A_2 are minimum and maximum of the Boltzmann curve, respectively. Each cell tested was individually fit to Equation 2.

Current density (J) is the measure of the current normalized to the membrane area and it is calculated dividing current amplitude by the whole-cell capacitance, assuming a specific membrane capacitance of 1µF.cm^{-2} (Ribeiro & Costa 2000). The average current density values obtained were plotted against the step command pulse.

To study activation and inactivation kinetics of the recorded Na^+ currents, each trial of the activation protocol was fitted into an exponential curve, with the following Equation 3

$$i_t = \sum_{i=1}^{m} a_i e^{-t/\tau i} + c, \qquad \textit{Equation 3}$$

where τi is the time constant, a_i is the exponential amplitude coefficient, c is a constant. The activation phase was fitted into a single exponential ($m = 1$) and the inactivation phase was fit into a double exponential function ($m = 2$) with a fast and slow components; τ_i and a_i were noted. The average time constants obtained were plotted against the pulse command.

To study the voltage dependence of steady-state inactivation, the fraction of channels available for activation is obtained by normalization of the currents obtained at the command pulse to its maximum value (I/I_{max}). Values of normalized currents

were plotted against pre-pulse potentials, and data points from each cell were fitted with a sum of sigmoids, as in Equation 4:

$$\frac{I}{I_{max}} = \frac{a_1}{1 + \exp[(V_{Hfast} - V_m)/V_{S\,fast}]} + \frac{1 - a_1}{1 + \exp[(V_{H\,slow} - V_m)/V_{S\,slow}]} \qquad \textit{Equation 4}$$

where V_{Hfast} and $V_{H\,slow}$ are the half-activation potentials from the fast and slow components of steady state inactivation of Na^+ currents and $V_{S\,fast}$ and $V_{S\,slow}$ are the corresponding slopes and $a_1$is a fitting parameter.

The fraction of current recovered after inactivation was obtained with the normalized current amplitude of each test pulse to the current amplitude of the pulse with the biggest delay (3500ms) and plotted against the time between the pre-pulse and pulse. Data were fitted to a double exponential equation (Equation 5):

$$I/I_{3500} = a_{fast}[1 - \exp(-t/\tau_{fast})] + a_{slow}[1 - \exp(-t/\tau_{slow})] + d. \qquad \textit{Equation 5}$$

where I/I_{3500} is the fraction of current recovered, a_{fast} and a_{slow} are the fractions of the fast and slow components, respectively and τ_{fast} and τ_{slow} are the time constants for each recovery component.

3.4 Protein expression

3.4.1 Western blot

Dissected DRG ganglia were placed immediately in cold homogenization buffer (HB) containing (in mM): EDTA 1, Tris 50, NaCl 150 (pH 7.4) and a protease inhibitor cocktail (PIC, ROCHE®, Basel, Switzerland, according to the manufacturer instructions) at the proportion of 10 mg of tissue to 100µL of HB+PIC and stored at -80°C until required to processing.

Samples were homogenized with a manual homogenizer and incubated on ice for 30 – 40 minutes with lysis buffer (LB) 1% (w/v) sodium deoxycholate (DOC), 1% (w/v) nonited P-40 and 0.1% (w/v) sodium dodecyl sulphate (SDS). The lysate was centrifuged for 30 minutes at 12 000 rpm, at 4°C and the supernatants were collected. Total protein content was determined by the bicinchoninic acid (BCA) protein assay kit (Micro BCA Pierce Thermo®, 23235).

Total protein extracts were denaturated in Laemmli sample buffer containing (in % w/v): dithiothreitol (DTT) 0.77, Bromophenol Blue 0.01, glycerol 5, SDS 1.5 and TRIS-HCL(pH 6.8); by mixing in vortex and incubating 10 minutes at room temperature. 30 µg of total protein extracts were applied in a 7% SDS-Polyacrylamide gel electrophoresis and wet transferred to a nitrocellulose membrane.

Blots were blocked for 2 hours at room temperature in 5% skimmed milk in TRIS-buffered saline (TBS) with 0.1% of Tween 20 detergent (TBS-T 0.1%) prior to the incubation with primary antibodies overnight, at 4°C. The antibodies used were polyclonal anti-Nav1.7 (1:500, Alomone labs® ASC-008), polyclonal anti-Nav1.8 (1:500, Alomone labs® ASC-016) and as a loading control, the monoclonal anti-αtubulin (1:2000, Santa Cruz® SC 58666).

The blots were washed three times for 5 minutes in TBS-T 0.1% and incubated with the secondary antibody polyclonal goat anti-rabbit IgG (H&L) peroxidase conjugated (1:3000, Rockland® 611-1302) for 90 minutes at room temperature.

Membranes were washed in 0.1% TBS-T and incubated with enhanced luminol chemiluminescence reagents (Clarity ECL Bio-rad®) according to the manufacture instructions. The intensity of the signals was detected in a Chemidoc Molecular Imager (Chemidoc, BioRad®) and densitometry was performed using the Image lab software

(BioRad®). Densitometry measures obtained from Nav1.7 and Nav1.8 protein lanes were normalized to the loading control and compared in terms of fold increase of expression in relation to the expression of L4-L6 DRG neurons.

3.4.2 Immunohistochemistry

The rat was deeply anesthesiated with sodium pentobarbital (100mg/kg i.p.), laid in a supine position and transcardially perfused with saline solution followed by 4% paraformaldehyde (PFA, Sigma® P6148) in 0.1M phosphate buffered saline (PBS). The DRG ganglia from ipsilateral and contralateral sites of injury were removed as stated above and left overnight in 30% sucrose with 0.1M PBS/0.025% sodium azide. Tissues were stored in optimal cutting temperature (OCT) mounting medium (VWR® 00411243) at -80°C until processing. Cryosections of 8-10µm were mounted in poly-L-lysine glass coated slides (Sigma® P0425).

The cryosections were permeabilized with Triton-X 0.05% in PBS for 10 minutes at room temperature, washed three times with PBS and incubated in the blocking solution (bovine serum albumin (BSA) 5%, fetal bovine serum (FBS) 5% in PBS) for 1 hour. Slides were again washed in PBS and incubated in a moister chamber overnight at 4°C with a mixture of the following primary antibodies: polyclonal anti-Nav1.7 (1:600, Alomone labs® ASC-008), polyclonal anti-Nav1.8 (1:600, Alomone labs® ASC-016) and anti β-III-tubulin (1:600,Millipore-Chemicon®AB9354) diluted in the blocking solution. After extensive washing with PBS, slices were incubated 1 hour at room temperature with the secondary antibodies Alexa 568 donkey α-rabbit (1:500, Invitrogen® A10042) and Alexa donkey 488 α-mouse (1:500, Invitrogen® A-21202), washed in PBS and mounted with fluormount-G medium containing DAPI (eBioscience® 00-4959-52) for fluorescence confocal microscopy (Leica® CTR400). Images were acquired and processed in LAS AF software (Leica®).

3.5 Statistical analysis

Statistical analysis was performed with SigmaStat 3.5 (Systat Software Inc®).

Mean differences were compared by the nonparametric Man-Witney rank sum test, when samples did not have a normal distribution and by the parametric t-test, when it did have parametric distribution. Differences were not assumed as significant when $p>0.05$ and significant when $p<0.05$ and $p<0.01$. Results are presented as mean±S.E.M. (standard error of the mean) for a number of n samples.

4. Results

4.1 Animal behaviour

To access 'pain' in a rat, and even, quantify it, is a great challenge and also an extreme powerful tool as, in a study likes the present, allows to correlate individual specimens, conditions and experiments. Most importantly, it allows to validate and corroborate the study of mechanistic phenomena, combining the behavioural with electrophysiological and protein expression approaches, raising their biological significance. Hence, to 'detect and quantify pain', three different behavioural read outs were observe: spontaneous pain, mechanical and thermal sensibility. Data was compared in two groups, regarding inflammatory and neuropathic chronic pain: 1) ipsilateral CFA hind paw against contralateral CFA and naïve hind paws; 2) ipsilateral CCI hind paw against contralateral CFA and ipsilateral sham hind paws. A total of 36 animals were used: CFA (n=7); naive (n=5) CCI (n=13); Sham (n=11).

4.1.1 Spontaneous Pain

The observation of the number of vertical rearings performed by rats in the open field of the behavioural cage is a putative approach to assess the innate responses to spontaneous pain (Rutten et al. 2014). Here, the observation of rearings was always performed prior to the mechanical and thermal pain tests, i.e., during the habituation period. Since it is a non-invasive test, the habituation of rats is not jeopardized. The average vertical rearings from naïve (n=5), CFA (n=7), sham (n=8) and CCI rats (n=8) are presented in Figure 13 and in Table 4 from the Supplementary data section.

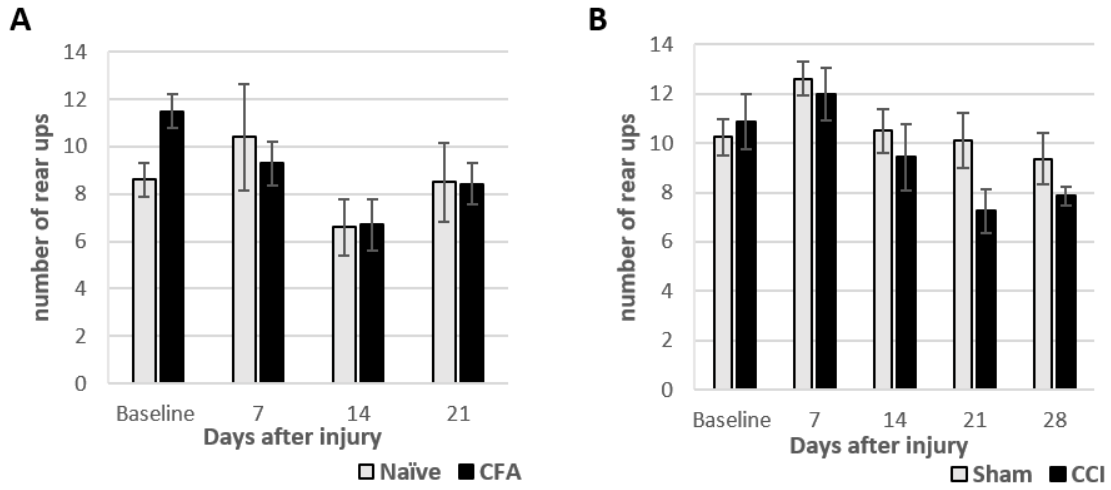

Figure 13 – Counts of vertical rearings in an open field from animals with inflammatory and neuropathic CP. A- In CFA rats (black bars, n=7) the average of vertical rearings was close to the average number of rearings performed by naïve rats (grey bars, n=5). **B**- In CCI rats (black bars, n=8), it is observed a lower average number of rearings, compared to sham (grey bars, n=8). However, the differences between groups are not statically significant ($p>0.05$; t-test). Vertical rearings values are summarized in Table 4, from Supplementary data. Error bars are given by S.E.M..

In the panel A of Figure 13, the average number of vertical rearings in CFA rats is similar to the mean vertical rearings of naïve rats, during the entire period of experiment. In panel B (Figure 13), it is observed that the induction of neuropathic pain by CCI model seems to reduce the average number of vertical rearings in rats, compared to its sham controls. Such differences became more obvious in the later stages of the experiment, but, however, the number of rear ups between pain model rats and its controls are not statistically significant ($p<0.05$; t-test).

The tendency observed suggests that CCI rats were more prone to fell spontaneous pain, in comparison with sham ones.

4.1.2 Mechanical sensibility

Following the establishment of the CFA and CCI pain models, mechanical sensitivity to evoked pain in the hind paw was observed using von Frey monofilaments (vFF). Figure 14 and Table 5 from Supplementary data depict the withdrawal thresholds from the ipsilateral hind paws to the site of injury. As mentioned before, the term ipsilateral hind paw is referred to the hind paw from the injured knee or

sciatic nerve, in the case of CFA or CCI, respectively. Such values are compared with the internal control (contralateral hind paws of injured rats, i.e., left uninjured hind paws) and with control rats (right hind paw from naïve and sham groups).

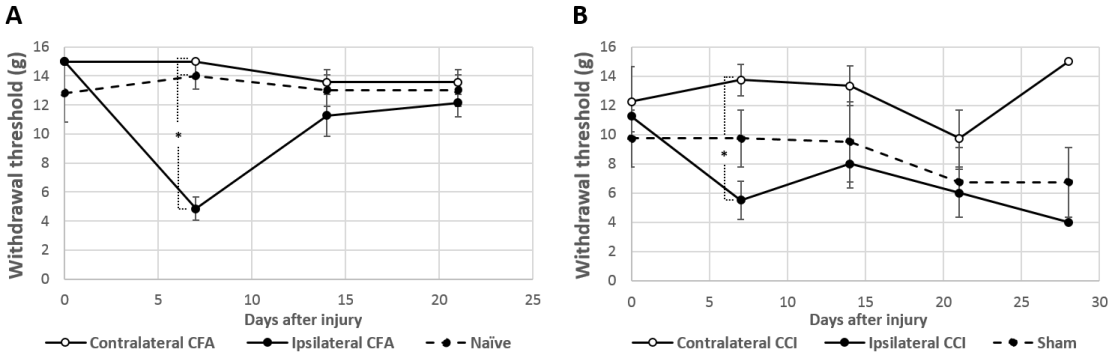

Figure 14 – Sensitivity to mechanical stimulation as a measure of hyperalgesia in CFA and CCI pain models. The average withdrawal threshold (defined as the weakest monofilament (g) that induced a pain behaviour in rats, (*see section 0 from Methods*) of contralateral paws (open dots), ipsilateral (filled dots) from pain model rats and respective controls (dashed line) are presented against the days after injury. **A**- CFA rats (n=7) had a significant hyperalgesic behaviour at the 7th day after injury, when compared to its contralateral hind paw and naïve rats (n=5), but it recovered some of its sensitivity and during the remaining time of the pain model. (*, p<0.01 vs contralateral and naïve; Mann-Whitney rank sum test) **B**- After the establishment of CCI, the ipsilateral hind paw from CCI rats (n=4) presented the lowest withdrawal threshold when mechanical stimulated, reaching its minimum at the 28th day after injury, when compared to its contralateral and sham (n=4) rats. Withdrawal responses values are summarized in Table 5 from Supplementary data. Error bars are given by S.E.M. (*, p<0.01 vs contralateral; t-test).

Analysing panel A from Figure 14, for the CFA pain model, at the baseline, the average withdrawal thresholds from all rats were similar: in the ipsilateral (n=7) and contralateral (n=7) paws from CFA rats values were 15±0g and in naïve rats (n=5), 12.8±1.97g. After seven days of induction of monoarthritis, the ipsilateral hind paw from CFA rats had a significant lower withdrawal threshold (4.85±0.79g), compared to both contralateral (15±0g) and naïve (14±0.89g) hind paws (p<0.01; Mann-Whitney rank sum test).

During the remaining weeks of the model, the withdrawal threshold values from CFA rats apparently recovered to baseline levels and showed withdrawal threshold values close to control hind paws. Concordantly, in the last day of the behavioural experiments, the CFA ipsilateral hind paws as well as the contralateral and naïve hind

paws presented similar withdrawal threshold values of: 12.14±0.94g, 13.57±0.85g and 13±1.10g, respectively.

The results indicate that CFA rats only developed secondary hyperalgesia at the 7th day post-injury.

The panel B from Figure 14, shows the withdrawal thresholds values obtained from experimental individuals of the CCI pain model. Data provides an idea of the progression of pain during the entire time of the behavioural experiment. At baseline, values from the different preparations were similar. In fact, the average withdrawal threshold from the ipsilateral hind paw (n=4) of CCI rats was of 11.25±1.08g, while contralateral (n=4) presented an average value of 12.25±2.38g and shams (n=4) a value of 9.75±1.95g. Seven days post-injury, however, the withdrawal threshold from CCI fell to 5.50±1.30g in the ipsilateral hind paw, which was significantly lower, compared to the contralateral hind paw (13.75±1.08g, $p<0.01$; t-test). In sham rats, the mechanical withdrawal threshold did not change in relation to baseline. At the fourteenth day after injury, CCI rats presented an apparent and moderate recovery in withdrawal thresholds, (8.0±1.63g), but still lower than the withdrawal threshold from the contralateral and sham hind paws, which remained the same range of values: 13.33±1.36g and 9.5±2.75g, respectively. At the twenty first day after injury, all rats showed a sudden higher sensibility (6.00±1.63g, 9.75±1.95g and 6.75±2.38g for ipsilateral, contralateral CCI and sham rats, respectively). The period between the 14th and 21stdays of this CCI model was coincident to construction work at the rodent house, which may be the cause for the increase in sensibility even in the control rats.

Finally, at the last day of mechanical sensibility assessment (28th day), withdrawal thresholds from the ipsilateral hind paw of CCI rats decreased to 4.00±0g, contrary to the contralateral hind paw that returned to baseline levels (15.00±0g) while sham rats remained at 6.75±2.38g of average hind paw withdrawal thresholds. Hence, overall, after one week after the start of experiment, the ipsilateral hind paws from CCI rats showed lower threshold values when compared with contralateral and sham hind paws, tendency observed throughout the experiment. Suh difference was less noticeable when compared with the sham.

4.1.3 Thermal sensibility

As stated above, the development of secondary thermal hyperalgesia is not described in inflammatory pain models, therefore cold allodynia was only tested rats integrating the neuropathic CCI pain model.

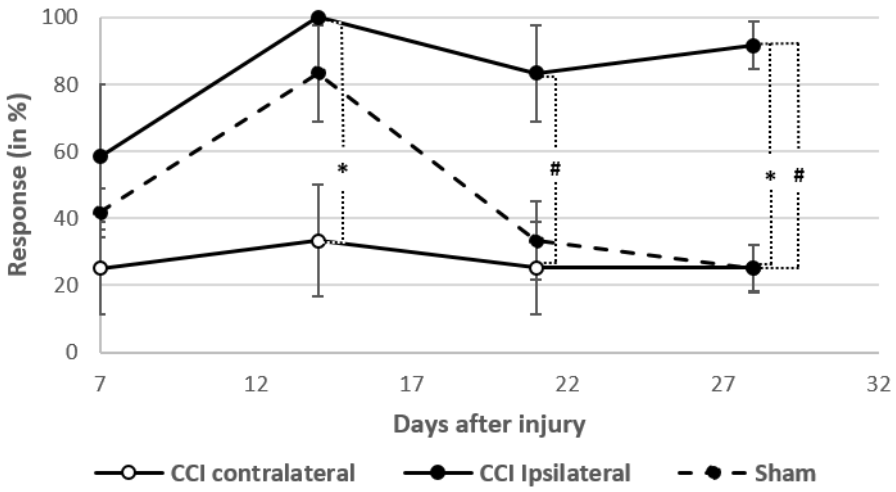

Figure 15 – Development of cold allodynia for the CCI pain model under study. The ipsilateral injured hind paw from CCI rats (n=4), at the 7th day after injury, had a similar but still higher sensibility to cold stimulus (58% ± 22), when compared to contralateral (25% ± 14) and sham (n=4; 42% ± 7) hind paws. At the 14th day of progression of the pain model, the ipsilateral hind paw had a significant higher sensibility (100%±0) in response to acetone, in comparison to the contralateral hind paw (33%±17) (*, $p<0.05$ vs contralateral; Mann-Whitney rank sum test). At the 21st day, the sensibility from CCI ipsilateral hind paw was significantly higher than contralateral hind paws (#, $p<0.05$ vs contralateral, t-test) and at the 28th day it was significantly higher than both contralateral and sham hind paws (*, $p<0.05$ vs sham, Mann-Whitney rank sum test; #, $p<0.05$ vs contralateral, t-test). Percentages of response values are summarized in Table 6 from supplementary data. Error bars are given by S.E.M.

Figure 15 and Table 6 from Supplementary data depicts the percentages of positive responses for cold allodynia following acetone testing for CCI (n=4) and sham rats (n=4) during the entire progression of the model, due to experimental constrains, it was not possible to present baseline values, although those experiments were performed. In one hand, at the 7th after injury no statistically significant differences were observed among CCI and its controls, since the average positive response to acetone in CCI ipsilateral hind paw was 58%±22, 25%±15 in contralateral and 42%±7 in sham. On the other hand, at the 14th day after injury, it was observed an increase of positive responses in CCI hind paws (100%±0), which was significantly higher in

comparison to its contralateral (33%±17; $p<0.05$, Mann-Whitney rank sum test); sham rats presented an average of 83%±14 positive responses at the same day. At the 21st day after injury, the sensibility of ipsilateral hind paws from CCI rats (83%±14) was significantly higher, comparing to the sensibility of its contralateral hind paw (25%±14; $p<0.05$; t-test). Finally, at the 28th day after injury, CCI ipsilateral hind paws presented a significantly higher sensibility (92%±7), compared to both contralateral (25%±7; $p<0.05$; t-test) and sham (25%±7; $p<0.05$; Mann-Whitney rank sum test) hind paws.

The increase of pain related behaviour in response to a cold stimuli, observed in the CCI hind paws reflects the development of cold allodynia, a well-known symptom of chronic pain, this increase would probably be even higher, if the baseline sensibility was accounted in this experiment.

Overall, the behavioural data presented here, showed that the experimental design for the establishment of the neuropathic CCI model is well accomplished.

4.2 Electrophysiology: Na^+ currents in small DRG neurons

The high relevance of Na^+ currents in neuroexcitability makes the electrophysiology studies upon it mostly important. In this section, the biophysical properties of Na^+ currents were analysed to evaluate the influence of CP in the neuroexcitability of DRG neurons.

Only cell showing stable, with low run-down and access resistance were used, a total of 20 cells (naïve n=7; CFA n=4; sham n=3; CCI n=6) were recorded in the electrophysiological studies. Data was compared in two groups, regarding inflammatory and neuropathic chronic pain: 1) naïve DRG neurons against ipsilateral DRG neurons from CFA and 2) ipsilateral DRG neurons from sham rats against ipsilateral DRG neurons from CCI rats.

4.2.1 Voltage dependence of activation

As name denounces, voltage-gated Na^+ channels exhibit a conformation dependent to the voltage difference across the interior and exterior of cell membranes (Catterall et al. 2005).

To study the voltage dependence of activation of VGSC in small DRG neurons, whole-cell voltage-clamp experiments were performed, whereas the protocol illustrated in panel A from Figure 16 was elicited: from the -70mV of holding potential, there was a pre-pulse to -110mV to achieve full removal of inactivation before the stepping to command pulses ranging from -50mV to +40mV. Representative current traces from Na^+ currents of small DRG neurons from naïve (n=7), CFA (n=4), sham (n=3) and CCI (n=6) rats are showed in panel B (Figure 16).

The average peak current from every command pulses of the activation protocol was plotted against the membrane potential, giving the current-voltage (I-V) relations presented in panel C and D from Figure 16, for the inflammatory (CFA) and neuropathic (CCI) CP models, respectively. The average maximum current occurred at +10mV in all groups was, as following: in naïve DRG neurons, -1606±310pA; in CFA,

-1491±178pA; in sham DRG neurons, -1532±314pA; and, in CCI, -2755±332pA. The differences in the average maximum current between naïve and CFA and between sham and CCI were not statistically significant (p>0.05; t-test).

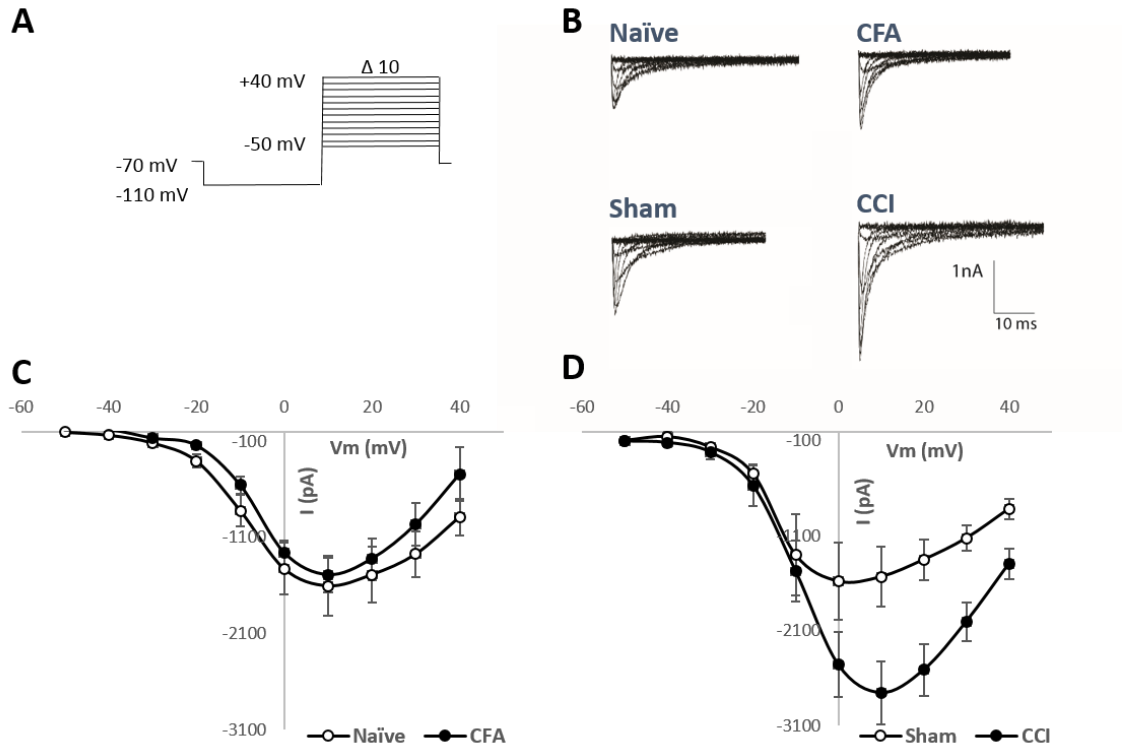

Figure 16 – Voltage dependence of activation of VGSC by whole-cell voltage-clamp recordings in small DRG neurons from inflammatory (CFA) and neuropathic (CCI) CP models. **A**- Activation protocol: Na^+ total currents were evoked by series of depolarizing command pulses from a holding potential of -70mV, followed by command pulses in steps of +10mV from -50mV to +40mV. Inactivation was removed with a pre-pulse of -110mV. **B**- Representative current traces of the activation protocol from small diameter DRG neurons of Naïve (n=7), CFA (n=4), Sham (n=3) and CCI (n=6) rats. **C** and **D**- Average current-voltage (I-V) relations from the inflammatory (**C**) and neuropathic (**D**) pain models (solid lines are presented for a better observation of data). **C**- In naïve (open dots) small DRG neurons the average maximum Na^+ current was approximately -1606±310pA and in CFA (filled dots) it was -1491±178pA. **D**- In sham small DRG neurons (open dots) it was -1532±314pA and in CCI (filled dots) it was 2755±332pA. The differences in average maximum Na^+ current between naïve and CFA and between sham and CCI are not statistically significant (p>0.05; t-test). Errors and error bars are given in terms of S.E.M..

The data points from Figure 16 were converted into current density values (pA/pF) (Figure 17). As in the I-V relations (Figure 16), the average maximum peak of current density occurred at +10mV, with the exception of sham, which had the peak of current density at 0mV. In naïve small DRG neurons was of -198.7±92 pA/pF, which was similar to what occurred in CFA small DRG neurons (-151.4±36 pA/pF). Sham small

DRG neurons presented a current density of -117.9±21 pA/pF, a value smaller than the one from CCI (-259±69 pA/pF).

Despite the differences clearly observed in current densities between sham and CCI small DRG neurons, reflecting an increase in the overall current density values for DRG neurons derived from CCI rats (Figure 17, panel B), such differences did not show any significance in t-test direct comparisons ($p>0.05$; t-test). However, the identified tendency, might reach to a statistical difference when sample size is increased and it may relate to a higher excitability of small DRG neurons under neuropathic pain conditioning.

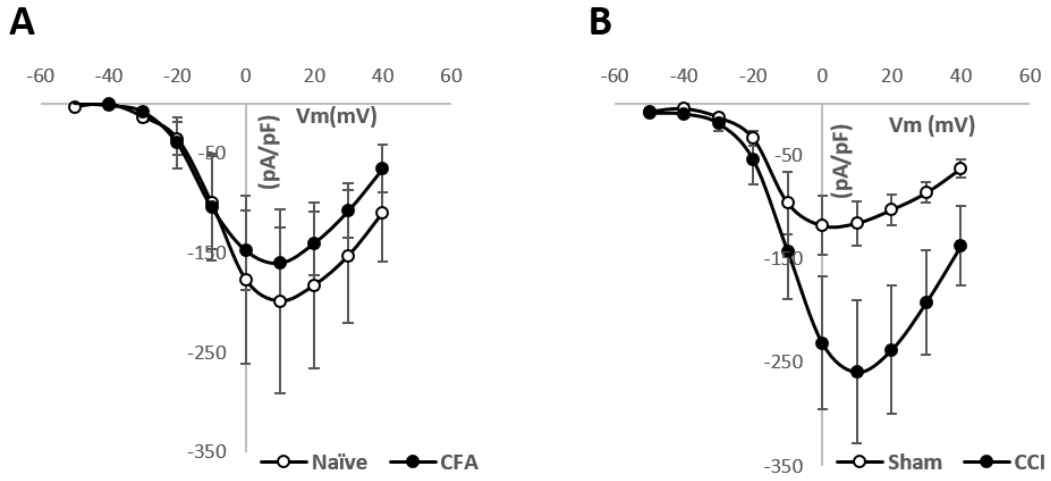

Figure 17 – Voltage dependence of current density of small diameter DRG neurons derived from CFA and CCI pain models. Na^+ current was normalized by cell capacitance as a measure of current density (pA/pF), solid lines from **A** and **B** are trend lines for a better comprehension of data. The average maximum peak of current density occurred at +10mV in the naïve (n=7), CFA (n=4) and CCI (n=6) groups and at 0mV in the sham group (n=3). **A**- In naïve DRG neurons (open dots), the average current density was of -198.7±92 pA/pF, similar to CFA (filled dots) -151.4±36 pA/pF. **B**- In sham DRG neurons (open dots) it was of -117.9±21 pA/pF and in CCI (filled dots) -259±69 pA/pF. The differences between the maximum values of current density between CFA and naïve and between sham and CCI small DRG neurons are not statistically significant ($p>0.05$; t-test). Errors and errors bars are given in terms of S.E.M..

To further study the voltage dependence of conductance of VGSCs in small DRG neurons from the pain models in study (*see Figure 18*) the current values from the IV plots (Figure 16) were converted in conductance values using the Equation 1, normalized to its maximum (G/G_{max}) and plotted against step pulse command. The data from each cell was fitted to Equation 2, where V_H represents the potential

necessary to activate half of the channel population and Vs reflects the channel response to a variation on the membrane potential.

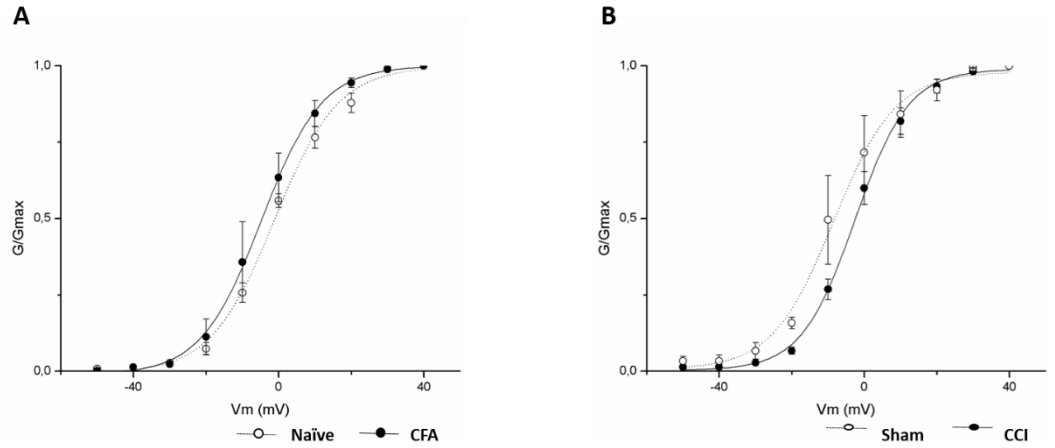

Figure 18 – Study of the voltage dependence of conductance of VGSC in small DRG neurons from CCI and CFA pain models, obtained from the I-V traces in Figure 16. A- Naïve DRG neurons (open dots, dashed line, n=5) had a V_H of -1.81±1.06mV and a V_S of 8.64±0.55mV, CFA DRG neurons (filled dots, continuous line n=3) had a V_H of -1.08±1.37mV and a V_S of 7.06±0.13mV, the differences among the described parameters were not statistically significant (V_H: p>0.05; t-test) and (V_S: p>0.05; Mann-Whitney rank sum test). **B**- In sham DRG neurons (open dots, dashed line, n=3), the average voltage dependence of activation had a V_H of -5.67±4.82mV and a V_S of 6.78±0.71mV, in the CCI small DRG neurons (filled dots, continuous line, n=6), V_H was of -2.85±1.58mV and V_S was of 7.93±0.70mV, as in the CFA pain model, the differences between V_H and V_S from the CCI and sham DRG neurons were not statistically significant (V_H: p>0.05; Mann-Whitney rank sum test) and (V_S: p>0.05; t-test). Error and error bars are given in terms of S.E.M..

The differences on fitting parameters V_H and V_S (±S.E.M.) among the various groups of small diameter DRG neurons are not statistically significant: naïve DRG neurons (n=5) had a V_H of -1.81±1.06mV and a V_S of 8.64±0.55mV, while CFA DRG neurons (n=3) had a V_H of -1.08±1.37mV (p>0.05; t-test) and a V_S of 7.06±0.13mV (p>0.05; Mann-Whitney rank sum test). In sham DRG neurons (n=3), average V_H was of -5.67±4.82mV and V_S was of 6.78±0.71mV, while the CCI DRG neurons (n=6) had a V_H of -2.85±1.58mV (p>0.05; Mann-Whitney rank sum test) and a Vs of 7.93±0.7mV (p>0.05; t-test). Therefore, the results indicate that the CP models studied did not induced any voltage shift on Na^+ currents present in DRG neurons from the models under study.

The absence of significant differences between the half voltage of activation (V_H) and the respective slope (V_S), from the Na^+ currents from small DRG neurons of the

pain models under study, leads us to conclude, that there were no alterations in the opening of activation gate of VGSC in response to an alteration in membrane potential. In other words, data shows data the assumed increase in neuroexcitability induced by nerve injury (CCI) is not mediated by a change in the voltage dependence of activation of VGSCs.

4.2.2 Voltage dependence of steady-state inactivation

The study of voltage dependence of steady-state inactivation allows the assessment of the fraction of channels available for activation at determined membrane potentials. The protocol used to perform this type of study is illustrated in Figure 19 (panel A): from the holding potential, a pre-pulse is elicited at the voltage which one intent to infer the voltage dependence of steady-state inactivation, followed by the command pulse to a voltage where full activation is obtained (+10mV). Series of pre-pulses ranging from -120mV to 0mV were tested (panel A from Figure 19). Representative current traces from the protocol are illustrated in the panel B (Figure 19) for all groups of small DRG neurons in study.

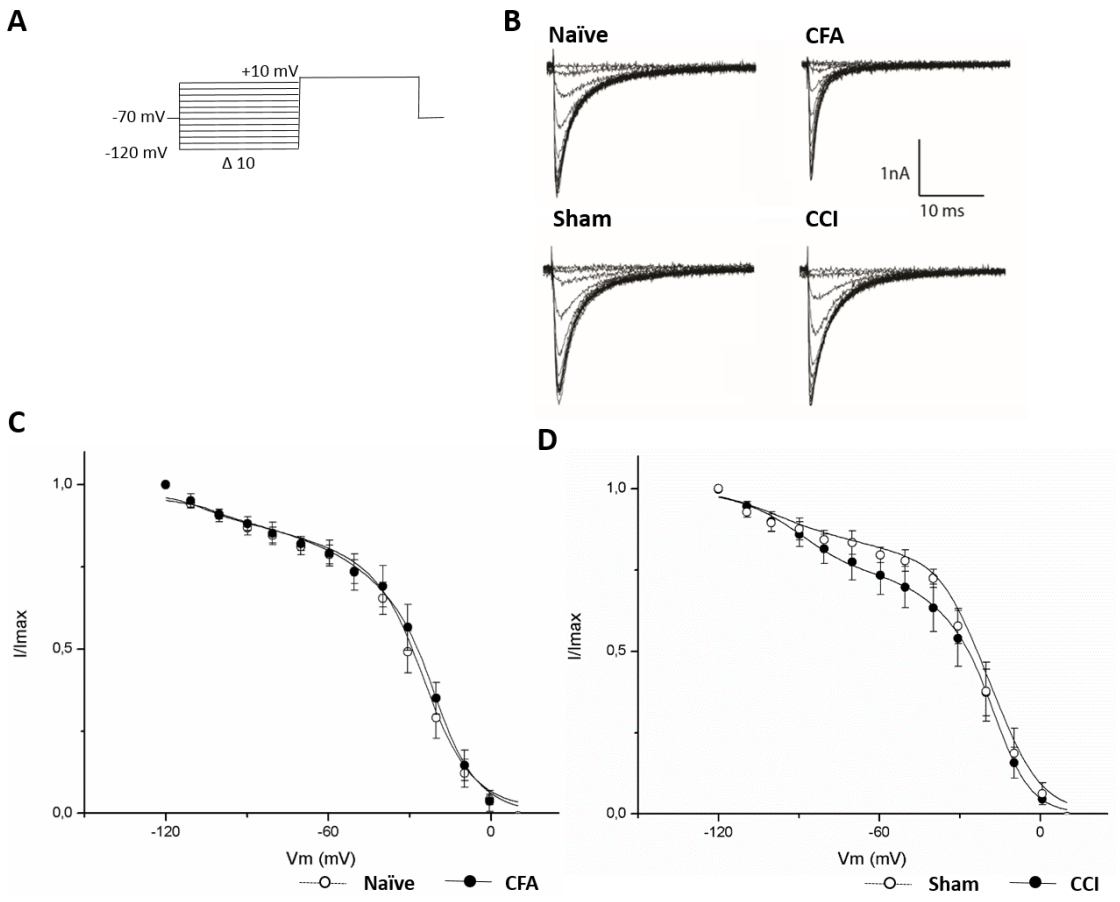

Figure 19 – Voltage dependence of steady-state inactivation of VGSC by whole-cell voltage-clamp recordings in small DRG neurons from CFA and CCI pain models. **A**- From the holding potential (-70mV), a pre-pulse ranging from -120mV to 0mV is elicited, followed by the command pulse to a voltage where full activation is obtained (+10mV). **B**- Representative current traces from naïve (n=6), CFA (n=3), sham (n=3) and CCI (n=6) DRG neurons when subjected to the protocol from A. **C** and **D**- Currents normalized to its maximum value (I/I_{max}), obtained at the command pulse, are plotted against the pre-pulse potentials. Data were fitted to Equation 4, average fitting parameters (V_H and V_S) from the fast and slow components of inactivation are present in Table 3. Error bar are given to S.E.M..

The fraction of channels available for activation is obtained by normalization of the currents obtained at the command pulse to its maximum value (I/I_{max}). In Figure 19 (panels C and D), the average values of normalized currents are plotted against pre-pulse potentials for the CFA and CCI pain models, respectively.

Data from each cell tested was better fit with a double exponential (Equation 4), maybe because in small DRG neurons there are two different channel populations of VGSC: one TTX-sensitive with a rapid inactivation (fast component, at hyperpolarized potentials) and other TTX-resistant, with a slower inactivation state (slow component, at more depolarized potentials) (Cummins & Waxman 1997). The relative contribution

of each component of Na^+ currents was estimated by the inflection point in the steady-state curves, as it was performed by other researchers (Cummins & Waxman 1997). From the observation of both panels C and D from Figure 19, it is clear that in the case of CFA pain model, there are no differences in the relative contributions of TTX-sensitive and TTX-resistant Na^+ currents from DRG neurons of naïve and CFA rats; while in the neuropathic pain model, it is not possible to rule an evident conclusion, although one may feel more willing to assume, due to the magnitude of the error bars, that the relative amount of Na^+ currents is not altered under neuropathic pain.

The average parameters for voltage of half inactivation and slopes from the fast and slow components of steady-state inactivation obtained are presented in Table 3, for naive (n=6), CFA (n=3), sham (n=3) and CCI (n=6) small DRG neurons.

Table 3 – Average fitting parameters of obtained for the study of voltage dependence of steady-state inactivation on small DRG neurons from the inflammatory (CFA) and neuropathic (CCI) pain models. Data was fit to Equation 4, the differences between the fitting parameters *($V_{H\,fast}$, $V_{S\,fast}$,$V_{H\,slow}$,* and $V_{S\,slow}$*)* of naïve (n=6), CFA (n=3) and between sham (n=3) and CCI (n=6) rats are not statistically significant (p>0.05; t-test).

	$V_{H\,fast}$	V_{Sfast}	$V_{H\,slow}$	V_{Sslow}
Naïve	-86.33±6.58	-7.17±6.96	-25.46±2.30	-7.25±0.91
CFA	-84.12±10.48	-13.08±2.99	-19.84±2.69	-6.99±0.76
Sham	-75.25±14.66	-14.67±0.55	-12.85±0.64	-8.58±1.58
CCI	-78.82±8.84	-13.41±1.29	-20.45±3.83	-6,11±0.26

The absence of statistically significant differences for the fitting parameters in the inflammatory pain (p>0.05; t-test) and in the neuropathic pain models, ($V_{H\,fast}$, $V_{H\,slow}$, p>0.05; t-test and $V_{S\,fast,}$, $V_{S\,slow}$; p>0.05; Mann-Whitney rank sum test), indicate that the inactivating gate from VGSC are not altered in the context of CP.

4.2.3 Recovery from inactivation

As mentioned in *section 0*, VGSC undergo a conformational cycle and therefore the study of the recovery from inactivation allows to assess the rate at which the channel can change, after its opening, from the inactive non-conductive state, to the initial closed state, ready to be activated again. The protocol used to study this feature of Na^+ currents is illustrated in the panel A of Figure 20: from the holding potential, cells were pre-pulsed to -110mV to achieve full removal of inactivation and pulsed to 0mV, for time enough to obtain full inactivation. The test pulses were elicited from -110mV to 0mV at different time points after the first pulse to 0mV; the delays varied from 0 to 3500ms. Representative current traces from the former protocol are depicted in panel B from Figure 20: it should be noted that Na^+ current represented is the current that ran through the channels that already recovered from the inactivated state at the second pulse.

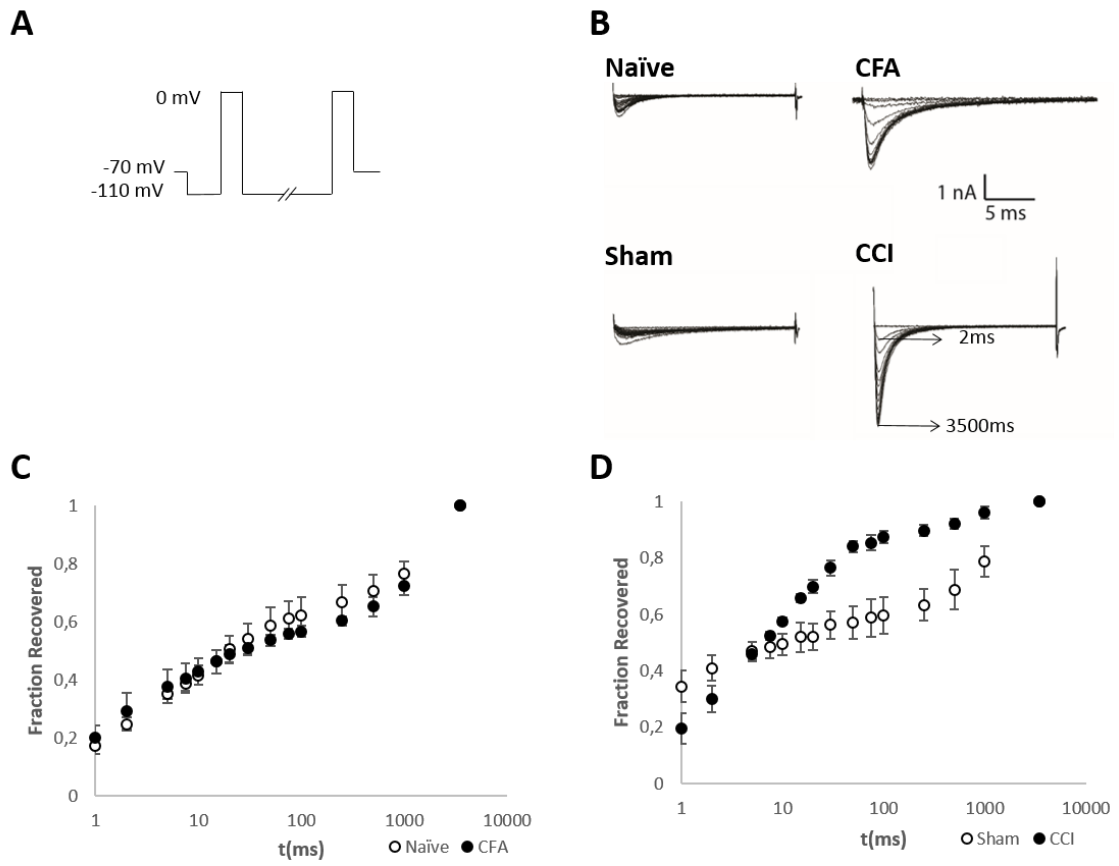

Figure 20 – Recovery from inactivation of VGSC, obtained by whole-cell voltage-clamp recordings, in small DRG neurons derived from the inflammatory and neuropathic rat pain models under study. A- From the holding potential (-70mV), recovery from inactivation was obtained by a pre-pulsed to -110mV to achieve full removal of inactivation of VGSC, followed by a short pulse to 0mV to obtain full

inactivation. The test pulses were elicited from -110mV to 0mV at different time points after the first pulse to 0mV; the delays varied from 0 to 3500ms. **B**- Representative current traces from naïve (n=6), CFA (n=4), sham (n=3) and CCI (n=3), derived small DRG neurons. The fraction of current recovered in smaller delays between pulses (e.g. 2ms) is smaller than the current recovered at higher delays (e.g. 3500ms) **C** and **D** - The fraction of current recovered represented as a function of time between pre-pulse and pulses. **C**- Naïve rats presented a τfast and τslow of 11.28±2.50ms and 2367±421ms, respectively; while CFA presented a τfast and τslow of 7.91±3.24ms and 18737±10201ms. **D**- Sham DRG neurons presented a τfast and τslow of 1.52±0.73ms and 1242±452ms, respectively. CCI small DRG neurons presented a τfast and τslow of 3.77±1.10ms and 45.56±6.00ms. The differences in a τfast between pain models and respective control were not statistically significant (p>0.05; t-test) as in τslow (p>0.05; Mann-Whitney rank sum test); errors and error bars are given in terms of S.E.M..

The average fractions of currents recovered, calculated by the normalization of the current observed at the second pulses to the current obtained in the pulse with the biggest delay (I/I_{3500ms}), is plotted against the time between both pulses in the panel C and D of Figure 20, for the inflammatory and neuropathic pain models, respectively. The fraction of current recovered from each cell tested was fitted with Equation 5 and the time of fast and slow recovery from inactivation was obtained.

In the inflammatory pain model, the time of fast and slow recovery from inactivation of Na^+ currents were similar in both pain model (CFA, n=4) and respective control (naïve, n=6). Specifically, in naïve small DRG neurons, τfast was 11.28±2.50ms and τslow, 2367±421ms; both values were not statistically different from those observed in CFA small DRG neurons, where τfast was of 7.91±3.24ms (p>0.05; t-test) and τslow was of 18737±10201ms (p>0.05; Mann-Whitney rank sum test).

When comparing sham results with CCI ones, one should analyse data in two instances: in what the smaller time interval between pre-pulse and pulse is concerned, currents from sham small DRG neurons (n=3) do not show a time of fast recovery from inactivation of Na^+ currents very different from CCI DRG neurons (n=3). In sham small DRG neurons, τfast was of 1.52±0.73ms, while in CCI DRG neurons, it was of 3.77±1.10ms, nevertheless, those differences in τfast are not statistically significant (p>0.05; t-test). When comparing time of slow recovery from inactivation, CCI small DRG neurons have a much smaller value of τslow (45.65±6.00ms), comparing to sham (1242±452ms), however as in τfast, the differences between sham and CCI DRG neurons in τslow were not statistically significant (p>0.05; Mann-Whitney rank sum test).

As in voltage dependence of steady-state inactivation, the fast and slow components of recovery from inactivation are thought to be attributed to different populations of VGSC (Cummins & Waxman 1997). Therefore, the tendency of a faster time of recovery from inactivation in the slow component observed might occurred in a specific VGSC isoform that at the moment, is not possible to identity, since we are observing total Na^+ currents. Nevertheless, the observed results are of utmost importance, because it gives valuable insights regarding the hyperexcitability of small DRG neurons in the context of CP.

Other biophysical parameters of currents were studied in the different pain models under study, such as the kinetics of activation and inactivation of Na^+ currents, although it did not presented conclusive results and therefore, were excluded from this section. Nevertheless, since the recovery from inactivation may relate to the kinetics of inactivation, the results from kinetics of inactivation from the CCI pain model are presented as supplementary data in Figure 23.

4.3 Nav1.7 and Nav1.8 expression on small DRG

The combination of electrophysiological studies with other biochemical techniques, such as immunohistochemistry and Western blot, allows to correlate the biophysical patterns of Na^+ currents measured at a molecular level, with the amount of channels expressed and stored in the cell. In this section will be presented results from immunohistochemistry and Western blot techniques from CFA and CCI pain models, relative to the expression of Nav1.7 and Nav1.8 proteins in DRG ganglia.

4.3.1 Immunohistochemistry

L5 and L6 DRG ganglia from a CFA rat (n=1) were studied to qualify the presence of the α-subunits of Nav1.7 and Nav1.8, as a preliminary assay for future directions of the present work. Due to the reduced sampling from this experiment, results are solely indicative and should be regarded warily.

Results of protein expression are presented in Figure 21, with panel A showing the study of Nav1.7, whilst panel B refers to Nav1.8.

In both experiments, since the β-III-tubulin is a marker of neuronal cells, one can conclude from the co-immuno-localization of the anti-β-III-tubulin and anti-Nav1.7 and Nav1.8 antibodies (see merge figures), that the expression of the Na^+ channels in study is confined to neuronal cells. For instance, no Nav1.7 or Nav1.8 staining was observed in non-neuronal cells, such as glial satellite cells.

In panel A from Figure 21, an apparent slight increase in Nav1.7 signal in ipsilateral DRG neurons may be observed. Regarding the study of Nav1.8 expression, images of the contralateral L5 and L6 ganglia are dimmer in comparison to the contralateral ones and probably the staining was not homogeneous for both slides. Therefore, it is not advisable to conclude about the relative expression of Nav1.8 from the presented results that require further research.

At the present moment, immunohistochemistry stainings for the CCI model are still being processed.

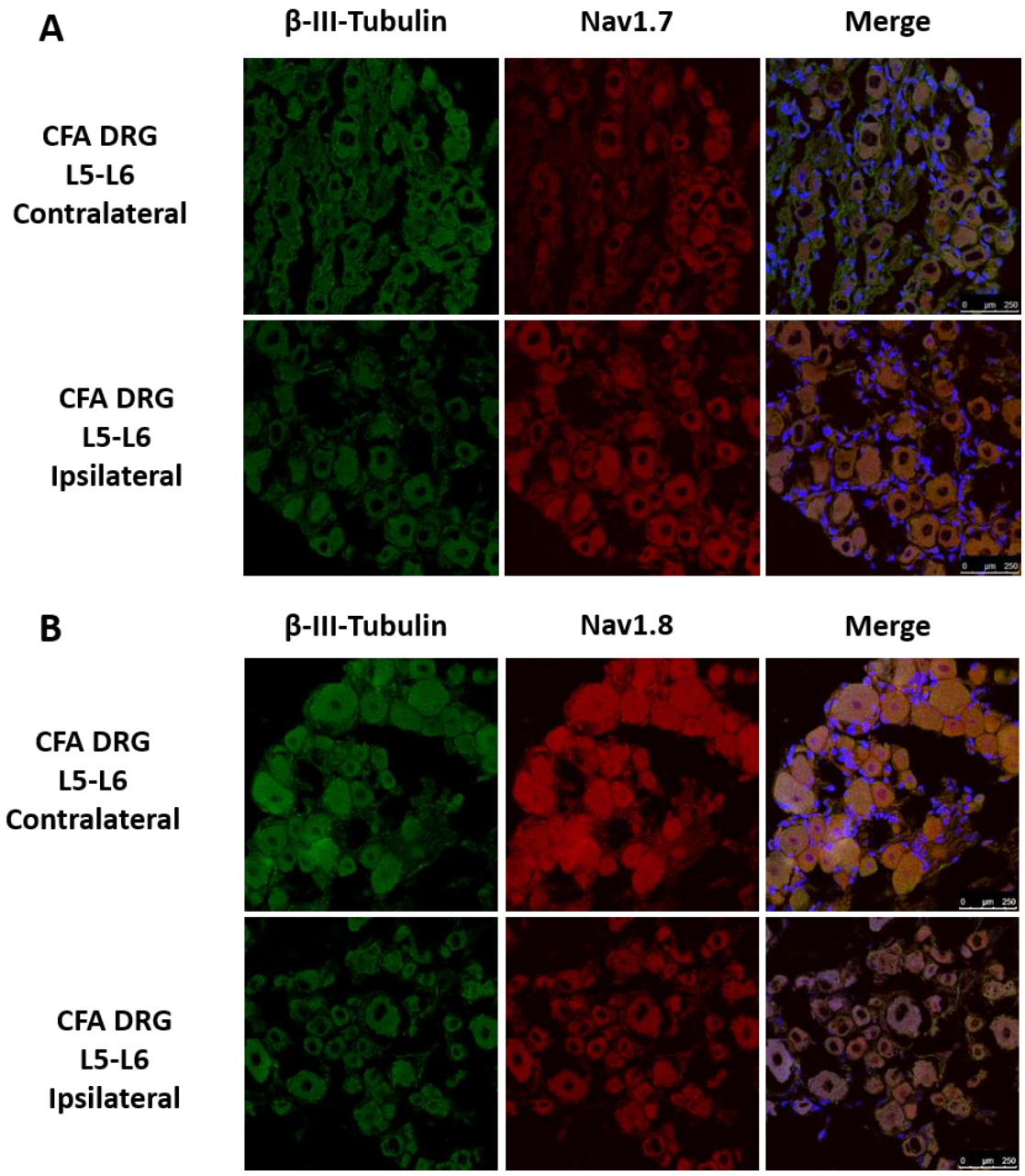

Figure 21 – Preliminary assays for the study of the influence of inflammatory chronic pain in the expression of Nav1.7 and Nav1.8 proteins in DRG neurons from contralateral and ipsilateral sites of injury (n=1). In both figures, the co-immuno-localization of the β-III-tubulin and the **(A)** Nav1.7 and **(B)** Nav1.8 staining indicate that these VGSC show a restricted expression in the neuronal cells from the DRG structure. For instance, no staining of Nav1.7 or Nav1.8 was observed in non-neuronal cells, such as glial satellite cells. Primary antibodies: polyclonal anti-Nav1.7 (1:600, Alomone labs® ASC-008), polyclonal anti-Nav1.8 (1:600, Alomone labs® ASC-016) and anti β-III-tubulin (1:600,Millipore Chemicon). Scale bar = 250 µm.

4.3.2 Western blot

In the neuropathic pain model (CCI), after the quantification of the total protein content in L4-L6 DRG ganglia from the contralateral and ipsilateral sites of injury, from sham (n=3) and CCI rats (n=2), samples of 30µg of total protein were analysed to its content of Nav1.7 and Nav1.8 channels by Western blot (Figure 22).

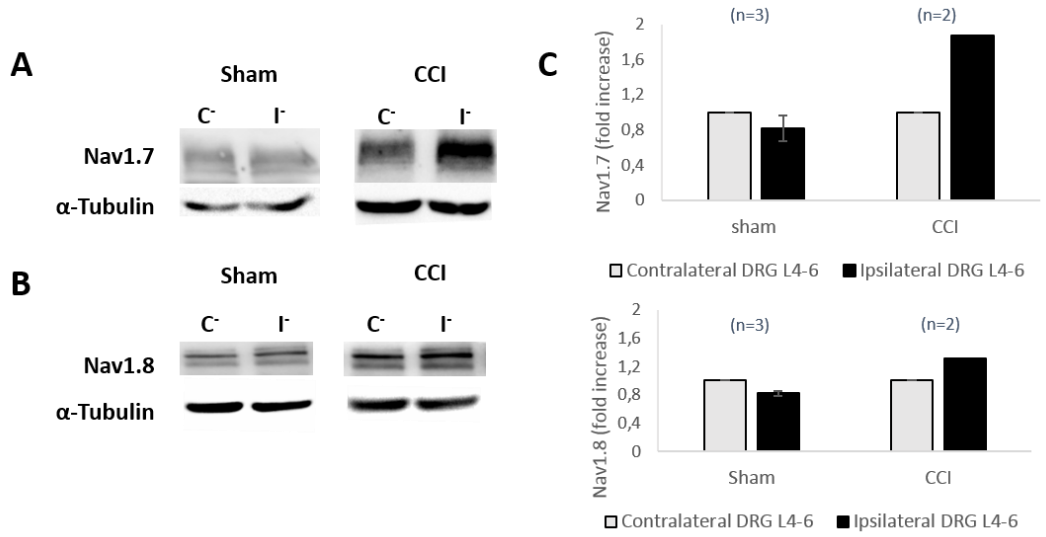

Figure 22 – Expression of Nav1.7 and Nav1.8 proteins in DRG ganglia from CCI and sham rats. A and B- Representative results of the assessment of Nav1.7 **(A)** and Nav1.8 **(B)** with polyclonal anti-Nav1.7 (1:500, Alomone labs® ASC-008) and polyclonal anti-Nav1.8 (1:500, Alomone labs® ASC-016) antibodies. As a loading control, the monoclonal anti-α tubulin (1:2000, Santa Cruz® SC 58666) antibody was used. **C**- Quantification of the fold increase in protein expression: Nav1.7 presented a fold increase of 0.81±0.15 in sham and 1.88 in CCI ipsilateral (I^-) DRG ganglia, compared to the contralateral (C^-) side; while Nav1.8 presented a fold increase of 0.88±0.03 in sham and 1.31 in CCI ipsilateral DRGs, compared to the contralateral side. Errors and error bars in sham are given in terms of S.E.M., no error bars are attributed to CCI rats due to the sample size (n=2).

Representative blots from the samples tested are shown in panels A and B from Figure 22. After normalization to the internal loading control (α-Tubulin), the fold increase of Nav1.7 and Nav1.8 in ipsilateral samples to the respective contralateral site of injury, or sham surgery, was obtained. Panel C from Figure 22 presents the average fold increases observed for the DRG ganglia from sham and CCI rats. No differences were observed between contralateral and ipsilateral DRG ganglia derived from sham rats for both Nav1.7 and Nav1.8 total protein expression.

On the other hand, one can observe an increase in the expression of Nav1.7 and Nav1.8 in the DRG ganglia from the ipsilateral site of injury of CCI, compared to the contralateral site. The average fold increase from the ipsilateral to contralateral ganglia was of 1.88 in Nav1.7 and 1.31 in Nav1.8, (no error values are presented due to the reduced sample size; n=2). This requires further tests for clarification.

Further Western blot analyses will still be performed concerning the expression of Nav1.7 and Nav1.8 in the CFA model.

Nevertheless, the expression levels of Nav1.7 and Nav1.8 are similar in the preparations from ipsilateral and contralateral DRGs of the sham rats. This indicates that the VGSCs are in fact dynamic and can be modulated in the context of chronic pain.

5. Discussion

The experiments performed and presented in the present dissertation give valuable insights to the physiopathology of Chronic pain. Overall, injured rats exhibited an altered behaviour, due to the induction of CFA and CCI pain models, in comparison to its controls. Moreover, it was also observed an abnormal function and expression of VGSC in DRG neurons following those pain models.

5.1 Neuropathic and inflammatory pain induced behavioural changes in rats

The appearance of spontaneous pain is a common consequence of CP. In the present work, the development of spontaneous pain was assessed in both inflammatory (CFA) and neuropathic (CCI) pain models by observation of the number of rearings that rats performed in the open field of the behavioural cage. It was expected to observe a reduction in the number of times that injured rats (CFA and CCI) reared up in the open field, in comparison to their controls (Rutten et al. 2014). Regarding the inflammatory pain model, CFA rats did not show a significant reduction in the number of rearings compared to the naïve controls. In the neuropathic pain model (CCI rats), although the results showed a tendency to the reduction on rear ups in injured rats, this difference was not significant. Nevertheless, the lower number of rearings observed in CCI rats leads to assume that these rats were more likely to experience spontaneous pain, compared to sham. Still, such behavioural readout appears to be less robust in comparison with the vFF, as discussed below.

Other research groups have identified the appearance of spontaneous pain in CCI injured rats, by observing repeated shaking, guarding and linking of the injured paw (Austin et al. 2012). Although those behaviours were not quantified in the present work, they were also observed in the CFA and CCI rats tested.

Mechanical hyperalgesia, which is also a common symptom of CP, can be assessed by the evoked withdrawal of the rat's paw, when stimulated by von Frey monofilaments (vFF) with different weight bending forces. In CFA rats, the marked decrease in paw withdrawal threshold at the 7th day post injury is a consequence of the development of secondary hyperalgesia. These results are corroborated with consistent observations from other researchers in a very similar inflammatory CFA pain model (Borzan et al. 2010). However, as the model progressed, the average ipsilateral hind paw sensibility to pain from CFA rats was recovered as animals presented a similar withdrawal threshold to its contralateral hind paw and naïve controls at 21st day post-injury. The duration chosen in the present work to study the processes of chronification of inflammatory pain with CFA is rare, therefore, there are not many experiences to compare with. Some other authors have also studied the development of hyperalgegia on rats subjected to an injection of CFA, up to 28 days (Goff et al. 1997). Goff and collaborators (1997) began to observe a recovery of mechanical sensibility in response to mechanical stimulation from the 4th day after injury, which support the findings showed here. Based on this change in behaviour, it would probably be advisable, as a future direction, to study the hyperalgesia phenomena and its consequences at the molecular level (i.e.: electrophysiology and biochemistry assays) with a shorter time of CFA induced pain progression. Alternatively, it may be also useful to use the hyperalgesic priming method to study CP, in which a transient insult with an inflammatory nature is performed before the insult that triggers the development of CP (Reichling & Levine 2009).

Chronic constriction of the sciatic nerve can induce an abnormal position on the hind paw of rats, which was suggested to be a consequence of dysesthesia or spontaneous pain (Attal et al. 1990). Moreover, the types of suture materials used for CCI of the sciatic nerve influence the hind paw position in different ways (Kajander et al. 1996). For instance, when the loose ligations are performed with chromic gut, rat toes are held together, plantar-flexed and the paw is everted (Austin et al. 2012). Therefore, measurements of hyperalgesia in CCI pain models are very demanding from the point of view of the experimenter. It should be noted tough, that, as in CFA, CCI rats were able to stand in both hind paws and walk through the cage easily. This is an

indication that the amount of pain induced in rats did not reach to humane endpoints in laboratory animal experiments.

In the CCI neuropathic pain model, seven days after injury, the average withdrawal threshold from ipsilateral hind paws of CCI rats was significantly lower in comparison to the withdrawal threshold of the contralateral hind paws, revealing that CCI rats developed mechanical hyperalgesia. However, the sensibility of CCI ipsilateral hind paws was partially recovered 14 days after injury. These observations are in accordance with previous works, as some have observed the beginning of the recover process at 14th day after injury in CCI rats (Liu et al. 2012; Novakovic et al. 1998).

Twenty-eight days after injury (end of the progression of the pain model), although not statistically significant, the ipsilateral sensibility of CCI rats showed again a higher sensibility, when compared to sham and, even more, when compared to their contralateral hind paws. Still important to mention here is that when animals were sacrificed, neither an absorption of the chromic gut suture or a regeneration of the sciatic ipsilateral nerves from CCI rats were observed. Therefore, the higher sensibility observed might be a consequence of the ongoing sensitization of nerve fibers in this particular CCI model.

The development of cold allodynia was evident from the 14^{th} to the 28^{th} day after injury in the ipsilateral hind paw from CCI rats, since they presented a higher sensibility to the cold stimulus, comparing to contralateral and sham hind paws. Similar results were obtained from the study on CCI pain model of Novakovic (1998). (Novakovic et al. 1998).

Hence, taken the behavioural readouts as whole, the protocol (and the time span) used for CCI appears to be adequate, a conclusion that is reinforced when cross examined with the functional data (see below).

5.2 VGSC expression might be affected in inflammatory chronic pain

The magnitude of the current running through a biological membrane depends on the density of channels, the conductance of the open channel and how often the channel spends in its open position and also its open probability (Bezanilla 2000).

From the whole-cell voltage-clamp recordings, results did not show any significant alteration in the biophysical properties of Na^+ currents in small diameter DRG neurons isolated from CFA rats in comparison to the naïve ones, 21 days post-injury. Nevertheless, it should be noted that previous works concerning inflammatory pain in shorter time courses reported an increase in total Na^+ current from TTX-sensitive and TTX-resistant channels, as well as an increase in the current density (Black et al. 2004; Wang et al. 2007; Tanaka et al. 1998). Since it was observed a reduction in secondary hyperalgesia assessed by vFF with the progression of the CFA model that could be translated into a recovery in their sensibility, it is postulated here that this initial state of hyperalgesia was a consequence of inflammation, which disappeared overtime. Considering what has been discussed before about hyperalgesic priming (Reichling & Levine 2009), it is possible that, under the protocol of inflammatory CP used, we were just inducing priming and not long term changes. This could be one of the reasons behind the lack of differences in biophysical properties of Na^+ currents between CFA and naïve neurons.

On the other hand, the afferents enervating the knee from rats, namely the saphenous and sciatic nerves, have their cell bodies in the DRG from L3 to L5 vertebrae's (Strickland et al. 2008). Here, it was collected DRGs located only within L4 to L6 vertebrae for electrophysiology recordings, and thus the contamination with the L6-DRG neurons and the lack of L3-DRG neurons may also contribute to the non-significant differences in Na^+ currents biophysical properties between naïve neurons and CFA-derived neurons under study.

In the immunohistochemistry assays, it was observed that the expression of Nav1.7 and Nav1.8 was confined to neuronal cells within the DRG, which is in accordance with the earlier observations (Dib-Hajj et al. 2012). Previous studies in knee CFA inflammatory pain models have demonstrated, by immunohistochemistry,

an increase in Nav1.7, Nav1.8 (as well as Nav1.9) proteins expression in small DRG neurons until the 28th day post CFA injection (Strickland et al. 2008). Others have observed, an increase in the expression of Nav1.7 and Nav1.8 proteins in the ipsilateral DRG in comparison to the contralateral DRG by both immunohistochemistry and Western blot (Black et al. 2004). These findings support the immunohistochemistry observations reporting Nav1.7 protein expression regarding the CFA rat.

The apparent contradictory results from the electrophysiology studies that did not evidence an altered function in VGSC in CFA small DRG neurons and immunohistochemistry that evidence and altered expression of Nav1.7, may not be an actual contradiction, since it is possible to have an overall increased protein expression without having a more functional protein. From the immunohistochemistry it is not possible to discriminate the functional state of the channel, but only assess its localization, amount of expression or association with other cellular components or proteins. Moreover, this are preliminary results where immunohistochemistry was performed with tissues collected from only one CFA rat, and, thus, such results should be regarded warily.

5.3 The function and expression of VGSC is altered in neuropathic CP

The analysis of biophysical properties of Na^+ currents in isolated small diameter DRG neurons showed a tendency of Na^+ current density to be relatively increased in CCI neurons in comparison to sham ones. This increase in current density was not due to a change in the voltage dependence of activation (and inactivation), which, lead to a mechanist explanation involving solely an increase of number of channels or increase of single channel conductance. Moreover, higher rate of slow recovery from inactivation in CCI small diameter DRG-neurons implies that the overall voltage-gated ion channels can change from the inactive to the closed state faster at more spaced pulses and therefore are more able to support repetitive firing frequencies (Dib-Hajj et al. 2009; Herold et al. 2009). Alternatively, it could be due to faster inactivation kinetics, which, we couldn't detect (see Figure 23 from Supplementary data).

In the Western blot analyses from tissue samples of CCI and sham rats, a tendency of increase in the protein expression of Nav1.7 and Nav1.8 at the ipsilateral ganglia from L4 to L6 DRG was observed, when compared to the correspondent ganglia from the contralateral site of injury. Since in this experiment, the entire ganglia was being analysed, it is not possible to state with accuracy if the increase is specifically observed in small, medium or large DRG neurons. Also it is not possible to state if the increase in the cited VGSC occurs in the injured, uninjured or in both DRG neurons. This could be done in the future with immunohistochemistry assays showing co-localization of VGSC under study with, for example, protein markers for small-diameter neurons and for injured cells. Other groups have also identified an increase in Nav1.7 protein expression on DRG ganglia 28 days after CCI injury (C. Liu et al., 2012). Other immunohistochemistry studies from CCI rats have observed that 7 days after injury, the expression of Nav1.8 was lower in the ipsilateral small DRG neurons, being even more decreased at the 14th day after injury and it returned to basal values at 28 days after injury; there were no alterations identified in Nav1.8 expression in medium and large DRG neurons (Novakovic et al. 1998). Moreover, it has been described an upregulation of the Na^+ channel Nav1.3 and an downregulation of Nav1.8 in neuropathy resulting from axotomies (Cummins & Waxman 1997). On the other hand, Dong and collaborators (2007) have showed that a robust knockdown of Nav1.8 current *in vivo* (by siRNA delivered to lumbar DRG) was able to cause a significant reduction of Nav1.8 mRNA expression in L4-L5 DRG neurons and consequently reversed mechanical allodynia in CCI rats. Authors concluded that silencing of Nav1.8 channel using a siRNA approach is capable of producing pain relief in the CCI model and further support a role for Nav1.8 in pathological sensory dysfunction (Dong et al. 2007), which corroborates in part the presented findings regarding Nav1.8 expression in CCI rats.

Nevertheless, the majority of studies regarding similar CCI models, terminates at the 14th day post-injury (coincident with the lower withdrawal thresholds in animal behaviour experiences). In order to have a more pain chronicity in the studied model, results presented in this dissertation were obtained 28th day post-injury. Therefore, comparisons between the results obtained and the literature should take these factors

in account. Furthermore, the tightness of the not constriction performed in the sciatic nerves may have some variability, resulting in a different number ratio between injured and uninjured fibers (Austin et al. 2012), which also should be taken into account.

A previous report related to the expression of Nav1.8 and Nav1.9 over time in DRG neurons from neuropathic human patients. It showed that both channels are expressed in DRG neurons in physiological conditions. However, 4 to 8 days post-injury, the expression of both Na^+ channels is weak. And, weeks after injury, some of the expression becomes to recover. A year after the injury, the expression of Nav1.8 and Nav1.9 returns to basal levels (Coward et al. 2000). Therefore, the discrepancies reported between the obtained results and some of the results from previous reports are possibly due to the different endpoints from studies. The expression of Nav1.8 in 14 days neuropathic pain model might be more resembled to the expression at 4-8 days after injury in humans and the expression of Nav1.8 in 28 days might be correspondent to the 12 months human injured neurons, as it was observed by Novakovic and his colleagues (1998) (Novakovic et al. 1998).

The literature related to the study of the influence of neuropathic pain in Na^+ currents is controversial (Blum et al. 2002). Once in CP the small DRG neurons are in a state of hyperexcitability, one would expect to observe an increase in current density, as it was observed in the presented results from CCI rats and in previous reports in painful diabetic neuropathy (Sun et al. 2012) and inflammatory pain models, as stated above. However, some previous studies reported no significant changes in the Na^+ total current density from small DRG neurons from CCI rats (Novakovic et al. 1998); others, a decrease in both Na^+ current densities (Huang & Song 2008); and others reported an increase in TTX-sensitive Na^+ and a decrease in TTX-resistant Na^+ current density in DRG neurons following axotomy (Cummins & Waxman 1997). Considering these puzzling state-of-the-art, the present work, which aims to conduct comparative studies in both models, gain importance, raising our motivation to carry on further.

As mentioned in *section 1.3.1.3* from *Introduction*, both Nav1.8 and Nav1.3 have a rapid recovery from inactivation. Taking in account (1) the published results from other groups (Cummins & Waxman 1997), (2) the electrophysiology recordings

obtained here do not distinguish between VGSC isoforms and (3) the Western blot experiences were not designed to assess the expression of Nav1.3, one should consider the possibility that Nav1.3 channel was also upregulated in the DRG neurons from the CCI model, therefore influencing the times of recovery from inactivation obtained. However, the absence of variations in the relative contributions of TTX-sensitive and TTX-resistant Na^+ currents in the voltage dependence of steady-state inactivation does not indicate an upregulation of those currents (Dib-Hajj et al. 1999).

Nevertheless, in his review, Wang *et al* (2011) have reported that the blockage of the Nav1.3 by antisense oligo deoxynucleotides (ASO) did not improved consistently the hyperalgesic behaviour of rodents following nerve injury (Wang et al. 2011) and that on the same hand, Nav1.3 knock-out mice did not prevent the development of a neuropathic pain behaviour. On the other hand, the inhibition of Nav1.8 synthesis *in vivo* with ASO resulted in a reduction of the slow inactivating TTX-resistant current and promoted the regression of neuropathic pain behaviour in rats following a spinal nerve ligation (Lai et al. 2002).

Taken together the results from electrophysiology and biochemistry analyses, it is tempting to outline the following considerations: neuropathic pain due to the chronic constriction in the sciatic nerve induced an increase in the expression of functional Nav1.7 and Nav1.8 proteins, translated into a higher current density and a faster time of slow recovery from inactivation. Therefore, the development of a drug that target those outlined altered biophysical properties, restoring the basal functions of those channels, emerges as mostly valid strategy to tackle CP.

6. Conclusions

The present dissertation explored the physiopathology of CP in the context of two different aetiologies, inflammation and neuropathy.

The most promising results obtained rely in the tendencies observed in the neuropathic pain model (CCI pain model). It was observed a higher current density and a more rapid time of slow recovery from inactivation in the Na^+ currents recorded from small DRG neurons, which was partially corroborated by the observation of a higher expression of Nav1.7 and Nav1.8 in the DRG affected by the constriction injury. It is likely that such mechanisms may underlie the supposed increases of neuroexciatbility on the affected fibers.

Although the inflammatory pain model failed to identify biophysical changes in the Na^+ currents from small DRG neurons and taking in consideration the observations from the immunohistochemistry tendencies, leads to conclude that, with a fine tuning of the experimental design (*see Future directions, section 727)*, one will have a better understanding of the alterations in the excitability of nociceptive pathway during CP associated with inflammation.

Nevertheless, the obtained results gave key insights related to the altered features in the biophysics of Na^+ currents and the expression of Nav1.7 and Nav1.8 in CP and encourage to continue the research throughout this path. Most importantly, they add to the rational of making emerge as key targets for CP treatment.

7. Future directions

The obtained results provide important insights on the physiopathology of CP. However, additional experiments are needed to further validate DRG neurons as a pharmacological target, in particular the VGSCs that are changing following neural-inflammation and neuropathy. Specifically, the future directions will be focus on:

- Improve the inflammatory pain model, in order to guarantee that pain rat models are indeed in a Chronic pain condition. This could be performed by decreasing the time progression of the pain model or by using models of hyperalgesic priming with inflammatory substances (e.g. CFA).

- Add more behavioural read-outs such as the assessment of putative spontaneous pain postures (linking and flinching the hind paw), as well as weight bearing measures.

- Discriminate the contributions of different isoforms of VGSC in both electrophysiology and protein expression experiments. This will be accomplished by the use of specific blockers, such as TTX and ProTx-I (β-theraphotoxin-Tp1a; a specific blocker of Nav1.8 Na^+ currents) in the electrophysiology experiments and by using more antibodies against VGSC, particularly against Nav1.3, in immunohistochemistry and western blot experiments.

8. References

Akopian, a N., Sivilotti, L. & Wood, J.N., 1996. A tetrodotoxin-resistant voltage-gated sodium channel expressed by sensory neurons. *Nature*, 379(6562), pp.257–262.

Amaya, F. et al., 2006. The voltage-gated sodium channel Na(v)1.9 is an effector of peripheral inflammatory pain hypersensitivity. *The Journal of neuroscience : the official journal of the Society for Neuroscience*, 26(50), pp.12852–12860.

Amin, B. & Hosseinzadeh, H., 2012. Evaluation of aqueous and ethanolic extracts of saffron, Crocus sativus L., and its constituents, safranal and crocin in allodynia and hyperalgesia induced by chronic constriction injury model of neuropathic pain in rats. *Fitoterapia*, 83(5), pp.888–895.

Assotakis, L.A.K. et al., 1999. A comparison of the potential role of the tetrodotoxin-insensitive sodium channels , PN3 SNS and NaN SNS2 , in rat models of chronic pain. *Proceedings of the National Academy of Sciences of the United States of America*, 96(July), pp.7640–7644.

Attal, N. et al., 1990. Further evidence for “pain-related” behaviours in a model of unilateral peripheral mononeuropathy. *Pain*, 41(2), pp.235–51.

Austin, P.J., Wu, A. & Moalem-Taylor, G., 2012. Chronic Constriction of the Sciatic Nerve and Pain Hypersensitivity Testing in Rats. *Journal of Visualized Experiments*, (61), pp.1–6.

Azevedo, L.F. et al., 2012. Epidemiology of chronic pain: a population-based nationwide study on its prevalence, characteristics and associated disability in Portugal. *The journal of pain : official journal of the American Pain Society*, 13(8), pp.773–83.

Bagriyanik, H. a. et al., 2014. The effects of resveratrol on chronic constriction injury of sciatic nerve in rats. *Neuroscience Letters*, 561, pp.123–127.

Baron, R., 2006. Mechanisms of disease: neuropathic pain--a clinical perspective. *Nature clinical practice. Neurology*, 2(2), pp.95–106.

Bartley, E.J. & Fillingim, R.B., 2013. Sex differences in pain: a brief review of clinical and experimental findings. *British journal of anaesthesia*, 111(1), pp.52–8.

Basbaum, A.I. et al., 2009. Cellular and Molecular Mechanisms of Pain. *Cell*, 139(2), pp.267–284.

Belkouch, M. et al., 2014. Functional up-regulation of Nav1.8 sodium channel in Aβ afferent fibers subjected to chronic peripheral inflammation. *Journal of neuroinflammation*, 11, p.45.

Bennett, G.J. & Xie, Y.K., 1988. A peripheral mononeuropathy in rat that produces disorders of pain sensation like those seen in man. *Pain*, 33(1), pp.87–107.

Bezanilla, F., 2000. The voltage sensor in voltage-dependent ion channels. *Physiological reviews*, 80(2), pp.555–592.

Bird, E. V et al., 2013. Correlation of Nav1.8 and Nav1.9 sodium channel expression with neuropathic pain in human subjects with lingual nerve neuromas. *Molecular pain*, 9(1), p.52.

Black, J. a et al., 2004. Changes in the expression of tetrodotoxin-sensitive sodium channels within dorsal root ganglia neurons in inflammatory pain. *Pain*, 108(3), pp.237–247.

Black, J. a et al., 1999. Upregulation of a silent sodium channel after peripheral, but not central, nerve injury in DRG neurons. *Journal of neurophysiology*, 82, pp.2776–2785.

Blair, N.T. & Bean, B.P., 2003. Role of tetrodotoxin-resistant Na+ current slow inactivation in adaptation of action potential firing in small-diameter dorsal root ganglion neurons. *The Journal of neuroscience : the official journal of the Society for Neuroscience*, 23(32), pp.10338–10350.

Blum, R., Kafitz, K.W. & Konnerth, A., 2002. Neurotrophin-evoked depolarization requires the sodium channel Na(V)1.9. *Nature*, 419, pp.687–693.

Borzan, J. et al., 2010. Effects of soy diet on inflammation-induced primary and secondary hyperalgesia in rat. *European journal of pain (London, England)*, 14(8), pp.792–8.

Brackenbury, W.J. & Isom, L.L., 2011. Na+ channel β subunits: Overachievers of the ion channel family. *Frontiers in Pharmacology*, SEP(September), pp.1–11.

Brouwer, B. a et al., 2014. Painful neuropathies: the emerging role of sodium channelopathies. *Journal of the peripheral nervous system : JPNS*, 19(2), pp.53–65.

Campbell, J.N. & Meyer, R. a, 2006. Mechanisms of Neuropathic Pain Review. *Pain*, pp.77–92.

Cathy, R.M. & William, B.G., 1998. Chronic pain. *Annual review of medicine*, 49(1), pp.123–33.

Catterall, W. a, Goldin, A.L. & Waxman, S.G., 2005. International Union of Pharmacology. XLVII. Nomenclature and structure-function relationships of voltage-gated sodium channels. *Pharmacological reviews*, 57(4), pp.397–409.

Catterall, W. a., 2010. Ion channel voltage sensors: Structure, function, and

pathophysiology. *Neuron*, 67(6), pp.915–928.

Chaplan, S.R. et al., 1994. Quantitative assessment of tactile allodynia in the rat paw. *Journal of neuroscience methods*, 53(1), pp.55–63.

Clapham, D.E., 2003. TRP channels as cellular sensors. *Nature*, 426(6966), pp.517–524.

Costa, P.F., 1996. The kinetic parameters of sodium currents in maturing acutely isolated rat hippocampal CA1 neurones. *Brain research. Developmental brain research*, 91(1), pp.29–40.

Coward, K. et al., 2000. Immunolocalization of SNS/PN3 and NaN/SNS2 sodium channels in human pain states. *Pain*, 85, pp.41–50.

Cox, J.J. et al., 2006. An SCN9A channelopathy causes congenital inability to experience pain. *Nature*, 444(7121), pp.894–8.

Cummins, T.R., Howe, J.R. & Waxman, S.G., 1998. Slow closed-state inactivation: a novel mechanism underlying ramp currents in cells expressing the hNE/PN1 sodium channel. *The Journal of neuroscience : the official journal of the Society for Neuroscience*, 18(23), pp.9607–9619.

Cummins, T.R. & Waxman, S.G., 1997. Downregulation of tetrodotoxin-resistant sodium currents and upregulation of a rapidly repriming tetrodotoxin-sensitive sodium current in small spinal sensory neurons after nerve injury. *The Journal of neuroscience : the official journal of the Society for Neuroscience*, 17(10), pp.3503–14.

Dai, Y., 2015. *TRPs and pain*,

Decosterd, I. & Woolf, C.J., 2000. Spared nerve injury: An animal model of persistent peripheral neuropathic pain. *Pain*, 87, pp.149–158.

Denac, H., Mevissen, M. & Scholtysik, G., 2000. Structure, function and pharmacology of voltage-gated sodium channels. *Naunyn-Schmiedeberg's Archives of Pharmacology*, 362(6), pp.453–479.

Descalzi, G. et al., 2015. Epigenetic mechanisms of chronic pain. *Trends in Neurosciences*, 38(Box 2), pp.1–10.

Dib-Hajj, S. et al., 2002. NaN/Nav1. 9: a sodium channel with unique properties. *Trends in Neurosciences*, 25(5), pp.253–259.

Dib-Hajj, S.D. et al., 1999. Plasticity of sodium channel expression in DRG neurons in the chronic constriction injury model of neuropathic pain. *Pain*, 83, pp.591–600.

Dib-Hajj, S.D. et al., 2012. The NaV1.7 sodium channel: from molecule to man. *Nature Publishing Group*, (December), pp.1–14. 8/nrn3404.

Dib-Hajj, S.D., Black, J. a. & Waxman, S.G., 2009. Voltage-gated sodium channels: Therapeutic targets for pain. *Pain Medicine*, 10(7), pp.1260–1269.

Eijkelkamp, N. et al., 2012. Neurological perspectives on voltage-gated sodium channels. *Brain*, 135, pp.2585–2612.

Fan, N. et al., 2011. Increased Na+ and K+ currents in small mouse dorsal root ganglion neurons after ganglion compression. *Journal of neurophysiology*, 106(April 2011), pp.211–218.

Fukuoka, T. & Noguchi, K., 2011. Comparative study of voltage-gated sodium channel α-subunits in non-overlapping four neuronal populations in the rat dorsal root ganglion. *Neuroscience Research*, 70(2), pp.164–171.

Gilchrist, J., Olivera, B.M. & Bosmans, F., 2014. *Animal toxins influence voltage-gated sodium channel function.*,

Goff, J.R. et al., 1997. Reorganization of the spinal dorsal horn in models of chronic pain: Correlation with behaviour. *Neuroscience*, 82(2), pp.559–574.

Gold, M.S., Levine, J.D. & Correa, A.M., 1998. Modulation of TTX-R INa by PKC and PKA and their role in PGE2-induced sensitization of rat sensory neurons in vitro. *The Journal of neuroscience : the official journal of the Society for Neuroscience*, 18(24), pp.10345–55.

Habib, A.M., Wood, J.N. & Cox, J.J., 2015. Sodium channels and Pain. , 227.

Hains, B.C. et al., 2004. Altered sodium channel expression in second-order spinal sensory neurons contributes to pain after peripheral nerve injury. *The Journal of neuroscience : the official journal of the Society for Neuroscience*, 24(20), pp.4832–4839.

Harper, a a & Lawson, S.N., 1985. Conduction velocity is related to morphological cell type in rat dorsal root ganglion neurones. *The Journal of physiology*, 359, pp.31–46.

Herold, K.F. et al., 2009. Isoflurane inhibits the tetrodotoxin-resistant voltage-gated sodium channel Nav1.8. *Anesthesiology*, 111(3), pp.591–9.

Hille, B., 2001. *Ion Channels of Excitable Membranes* 3rd ed., Sinauer Associates, Inc.

Ho, C. et al., 2012. Differential Expression of Sodium Channel Subunits in Dorsal Root Ganglion Sensory Neurons. *Journal of Biological Chemistry*, 287, pp.15044–15053.

Ho, C. & O'Leary, M.E., 2011. Single-cell analysis of sodium channel expression in dorsal root ganglion neurons. *Molecular and cellular neurosciences*, 46(1), pp.159–166.

Hong, S. & Wiley, J.W., 2006. Altered expression and function of sodium channels in large DRG neurons and myelinated A-fibers in early diabetic neuropathy in the rat. *Biochemical and Biophysical Research Communications*, 339, pp.652–660.

Hori, Y. et al., 2013. Differential expression of rat hippocampal microRNAs in two rat models of chronic pain. *International Journal of Molecular Medicine*, 32(6), pp.1287–1292.

Huang, Z.-J. & Song, X.-J., 2008. Differing alterations of sodium currents in small dorsal root ganglion neurons after ganglion compression and peripheral nerve injury. *Molecular pain*, 4, p.20.

Hulse, R.P., Wynick, D. & Donaldson, L.F., 2011. Activation of the galanin receptor 2 in the periphery reverses nerve injury-induced allodynia. *Molecular pain*, 7(1), p.26.

Iyer, S. & Tanenberg, R.J., 2013. Pharmacologic management of diabetic peripheral neuropathic pain. *Expert opinion on pharmacotherapy*, 14(13), pp.1765–75.

Julius, D., 2001. Molecular mechanisms of nociception . *Nature*, 413(September), pp.203–210.

Kajander, K.C., Pollock, C.H. & Berg, H., 1996. Evaluation of hindpaw position in rats during chronic constriction injury (CCI) produced with different suture materials. *Somatosensory & motor research*, 13(2), pp.95–101.

Klugbauer, N. et al., 1995. Structure and functional expression of a new member of the tetrodotoxin-sensitive voltage-activated sodium channel family from human neuroendocrine cells. *The EMBO journal*, 14(6), pp.1084–90.

Krames, E.S., 2014. The Dorsal Root Ganglion in Chronic Pain and as a Target for Neuromodulation : A Review. , 2014.

Lai, J. et al., 2002. Inhibition of neuropathic pain by decreased expression of the tetrodotoxin-resistant sodium channel, NaV1.8. *Pain*, 95(1-2), pp.143–152.

Lampert, A. et al., 2010. Sodium channelopathies and pain. *Pflugers Archiv European Journal of Physiology*, 460, pp.249–263.

Lascelles, B.D.X. & Flecknell, P.A., 2010. Do animal models tell us about human pain? *Pain: clinical updates*, XVIII(5).

Liem, L. et al., 2013. A multicenter, prospective trial to assess the safety and performance of the spinal modulation dorsal root ganglion neurostimulator system in the treatment of chronic pain. *Neuromodulation : journal of the International Neuromodulation Society*, 16(5), pp.471–82; discussion 482.

Liu, C. et al., 2012. Nav1.7 protein and mRNA expression in the dorsal root ganglia of

rats with chronic neuropathic pain. *Neural regeneration research*, 7(20), pp.1540–4.

Liu, M. & Wood, J.N., 2011. The Roles of Sodium Channels in Nociception : *Pain*, pp.93–99.

Lopez-Santiago, L.F. et al., 2006. Sodium channel beta2 subunits regulate tetrodotoxin-sensitive sodium channels in small dorsal root ganglion neurons and modulate the response to pain. *The Journal of neuroscience : the official journal of the Society for Neuroscience*, 26(30), pp.7984–7994.

Malin, S. a, Davis, B.M. & Molliver, D.C., 2007. Production of dissociated sensory neuron cultures and considerations for their use in studying neuronal function and plasticity. *Nature protocols*, 2(1), pp.152–160.

Mansour, a. R. et al., 2014. Chronic pain: The role of learning and brain plasticity. *Restorative Neurology and Neuroscience*, 32(1), pp.129–139.

McCarter, G.C. & Levine, J.D., 2006. Ionic basis of a mechanotransduction current in adult rat dorsal root ganglion neurons. *Molecular pain*, 2, p.28.

Minett, M.S., Eijkelkamp, N. & Wood, J.N., 2014. Significant determinants of mouse pain behaviour. *PloS one*, 9(8), p.e104458.

Mogil, J.S., 2009. Animal models of pain: progress and challenges. *Nature reviews. Neuroscience*, 10(4), pp.283–294.

Nicholls, J.G.., Martin, A.R. & Wallace, B.G., 1992. *From Neuron to Brain* 3rd ed., Sinauer Associates, Inc.

Noda, M. et al., 1984. Primary structure of Electrophorus electricus sodium channel deduced from cDNA sequence. *Nature*, 312(5990), pp.121–7.

Novakovic, S.D. et al., 1998. Distribution of the tetrodotoxin-resistant sodium channel PN3 in rat sensory neurons in normal and neuropathic conditions. *The Journal of neuroscience : the official journal of the Society for Neuroscience*, 18(6), pp.2174–87..

O'Neill, J. et al., 2012. Unravelling the mystery of capsaicin: a tool to understand and treat pain. *Pharmacological reviews*, 64(4), pp.939–71.

Pope, J.E., Deer, T.R. & Kramer, J., 2013. A systematic review: current and future directions of dorsal root ganglion therapeutics to treat chronic pain. *Pain medicine (Malden, Mass.)*, 14, pp.1477–96.

Ramachandra, R. et al., 2013. NaV 1.8 channels are expressed in large, as well as small, diameter sensory afferent neurons. *Channels (Austin, Tex.)*, 7(1), pp.34–7.

Reichling, D.B. & Levine, J.D., 2009. Critical role of nociceptor plasticity in chronic pain. *Trends in neurosciences*, 32(12), pp.611–8.

Renganathan, M. et al., 2011. Contribution of Na v 1 . 8 Sodium Channels to Action Potential Electrogenesis in DRG Neurons Contribution of Na v 1 . 8 Sodium Channels to Action Potential Electrogenesis in DRG Neurons. , pp.629–640.

Ribeiro, M.A. & Costa, P.F., 2000. Kinetic parameters of calcium currents in maturing acutely isolated CA1 cells. *Developmental Brain Research*, 124(1-2), pp.11–23.

Rigaud, M. et al., 2008. Species and strain differences in rodent sciatic nerve anatomy: implications for studies of neuropathic pain. *Pain*, 136(1-2), pp.188–201.

Rush, A.M., Cummins, T.R. & Waxman, S.G., 2007. Multiple sodium channels and their roles in electrogenesis within dorsal root ganglion neurons. *The Journal of physiology*, 579, pp.1–14.

Rutten, K. et al., 2014. Burrowing as a non-reflex behavioural readout for analgesic action In a rat model of sub-chronic knee joint inflammation. *European Journal of Pain (United Kingdom)*, 18(2), pp.204–212.

Sandku, R., 2009. Models and Mechanisms of Hyperalgesia and Allodynia. , pp.707–758.

Shah, B.S. et al., 2001. Beta3, a Novel Auxiliary Subunit for the Voltage Gated Sodium Channel Is Upregulated in Sensory Neurones Following Streptozocin Induced Diabetic Neuropathy in Rat. *Neuroscience Letters*, 309, pp.1–4.

Shah, B.S. et al., 2000. Beta3, a Novel Auxiliary Subunit for the Voltage-Gated Sodium Channel, Is Expressed Preferentially in Sensory Neurons and Is Upregulated in the Chronic Constriction Injury Model of Neuropathic Pain. *European Journal of Neuroscience*, 12(11), pp.3985–3990.

Snell, R.S., 2006. *Clinical Neuroanatomy* 6th ed., Lippincott Williams & Wilkins.

De Sousa, M.V.P. et al., 2014. Building, testing and validating a set of home-made von Frey filaments: A precise, accurate and cost effective alternative for nociception assessment. *Journal of Neuroscience Methods*, 232, pp.1–5.

Strickland, I.T. et al., 2008. Changes in the expression of NaV1.7, NaV1.8 and NaV1.9 in a distinct population of dorsal root ganglia innervating the rat knee joint in a model of chronic inflammatory joint pain. *European journal of pain (London, England)*, 12(5), pp.564–72.

Sun, W. et al., 2012. Gastrodin inhibits allodynia and hyperalgesia in painful diabetic neuropathy rats by decreasing excitability of nociceptive primary sensory neurons. *PLoS ONE*, 7(6).

Tanaka, M. et al., 1998. SNS Na+ channel expression increases in dorsal root ganglion neurons in the carrageenan inflammatory pain model. *Neuroreport*, 9(6), pp.967–72.

Theile, J.W. & Cummins, T.R., 2011. Recent developments regarding voltage-gated sodium channel blockers for the treatment of inherited and acquired neuropathic pain syndromes. *Frontiers in Pharmacology*, OCT(October), pp.1–14.

Tsantoulas, C. & McMahon, S.B., 2014. Opening paths to novel analgesics: The role of potassium channels in chronic pain. *Trends in Neurosciences*, 37(3), pp.146–158.

Walz, W. et al., 2002. *Patch-Clamp analysis Advanced Techniques* 1st ed. W. Walz, A. A. Boulton, & G. B. Bake, eds., Humana Press Inc.

Wang, J.-G. et al., 2007. Local inflammation in rat dorsal root ganglion alters excitability and ion currents in small-diameter sensory neurons. *Anesthesiology*, 107(2), pp.322–332.

Wang, W. et al., 2011. Are voltage-gated sodium channels on the dorsal root ganglion involved in the development of neuropathic pain? *Molecular pain*, 7(1), p.16.

Waxman, S.G. et al., 2000. Voltage-gated sodium channels and the molecular pathogenesis of pain: a review. *Journal of rehabilitation research and development*, 37(October), pp.517–28.

Waxman, S.G. & Zamponi, G.W., 2014. Regulating excitability of peripheral afferents: emerging ion channel targets. *Nature neuroscience*, 17(2), pp.153–63.

Wood, J.N. et al., 2004. Voltage-gated sodium channels and pain pathways. *Journal of Neurobiology*, 61(April), pp.55–71.

Woolf, C.J. & Mannion, R.J., 1999. Neuropathic pain: aetiology, symptoms, mechanisms, and management. *Lancet*, 353(9168), pp.1959–64.

Woolf, C.J. & Salter, M.W., 2000. Neuronal plasticity: increasing the gain in pain. *Science (New York, N.Y.)*, 288(5472), pp.1765–1769.

Yu, F.H. & Catterall, W.A., 2003. Overview of the voltage-gated sodium channel family.

Yu, Y.Q. et al., 2011. Antisense-mediated knockdown of Nav1.8, but not Nav1.9, generates inhibitory effects on complete freund's adjuvant-induced inflammatory pain in rat. *PLoS ONE*, 6(5).

9. Supplementary data

Table 4 - Counts of vertical rearings in an open field from animals from naïve (n=5), CFA (n=7), sham (n=8) and CCI (n=8) rats, from the inflammatory and neuropathic pain models. Error bars are given by S.E.M..

	Naïve	CFA	Sham	CCI
Baseline	8.6±0.7	11.5±0.7	10.3±0.7	10.9±1
7th day	10.4±2.2	9.3±0.9	12.6±0.7	12±1.1
14th day	6.6±1.2	6.7±1.1	10.5±0.9	9.4±1.3
21st day	8.5±1.7	8.4±0.9	10.1±1	7.3±0.9
28th day	N/A	N/A	9.4±1	7.9±0.4

Table 5 – Hind paw mechanical withdrawal thresholds (in g) of naïve (n=5), CFA (n=7), sham (n=4) and CCI rats (n=4) from the inflammatory and neuropathic pain models, obtained by the stimulation with vFF. Values presented are means ± S.E.M..

	Naïve	CFA Contralateral	CFA Ipsilateral	Sham	CCI Contralateral	CCI Ipsilateral
Baseline	12.80±1.97	15.00±0	15.00±0	9.75±1.95	12.25±2.38	11.25±1.08
7th day	14.00±0.89	15.00±0	4.85±0.79	9.75±1.95	13.75±1.08	5.50±1.30
14th day	13.00±1.10	13.57±0.85	11.29±1.42	9.50±2.75	13.33±1.36	8.00±1.63
21st day	13.00±1.10	13.57±0.85	12.14±0.94	6.75±2.38	9.75±1.95	8.00±1.63
28th day	N/A	N/A	N/A	6.75±2.38	15.00±0	4.00±0

Table 6 – Average response values (in percentage) from the CCI (n=4) and sham (n=4) rats to cold stimulation with acetone. Errors are given by S.E.M..

	Sham	CCI Contralateral	CCI Ipsilateral
7th day	42±7	25±14	58±22
14th day	83±14	33±17	100±0
21st day	33±12	25±14	83±14
28th day	25±7	25±7	92±7

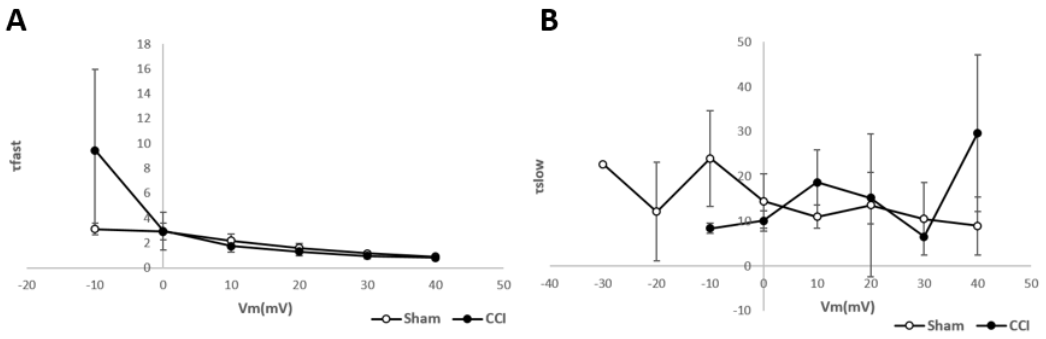

Figure 23 – Voltage dependence of inactivation from small DRG neurons from the CCI pain model. Average time constants of fast (**A**) and (**B**) slow inactivation from sham (n=3, open dots) and CCI (n=6, filled dots) small DRG neurons. Solid lines are presented for a better comprehension of data. Errors are given by S.E.M..